Automated Shape Sorting & Quality Mechanical Design

Abdelaziz Mohamed – 202300019

Ahmed Elrefaie – 202200083

Mazen Ammar – 202201133

Seif Samy – 202200404

Youssef Omran – 202200588

A project submitted to the faculty of the University of Hertfordshire in the New Administrative Capital in partial fulfillment of the requirements for the Integrated Engineering Systems Design - 5FTC2048 in the Mechanical Engineering and Mechatronics programme, School of Engineering and Computer Science

New Administrative Capital

2025-2026

Approved by:

Dr. Moataz Elsisy

Dr. Mohamed Nabil

ACKNOWLEDGMENT

We would like to express our heartfelt gratitude to Dr. Moataz Elsisy and Dr. Mohamed Nabil for their invaluable contributions and unwavering support throughout the journey of our team graduation project. Dr. Moataz Elsisy's guidance and expertise have been instrumental in shaping our project, providing us with valuable insights, and pushing us to strive for excellence. His dedication to academic excellence and commitment to our success have been a constant source of inspiration. Dr. Mohamed Nabil's practical knowledge and hands-on approach have significantly enriched our project. His mentorship, constructive feedback, and tireless efforts have played a crucial role in the successful execution of our team's goals. Their collaborative spirit, encouragement, and willingness to share their knowledge have been instrumental in the development of our skills and the overall success of our project. We are truly grateful for their mentorship and support.

Abstract

This project focuses on the design and development of an automated handling and sorting mechanism for industrial applications. The system is engineered to identify, move, and place objects based on predefined criteria such as size and shape. It integrates multiple subsystems—including a feeding station, conveyor belt, and rotating table, that work in synchronization to ensure efficient sorting and quality control. Key mechanical components such as the conveyor and rotating table are modeled using CATIA, and FEA is performed on ANSYS Workbench to predict load distribution, optimize durability, and minimize failure risks.

From an electrical perspective, the system incorporates motor drivers, power distribution circuits, and a variety of sensors, including proximity IR sensor, vision-based cameras to enable accurate object detection and actuation. Wokwi, which is a simulation website, was used to test the components with the required code. A microcontroller such as Arduino Uno manages real-time control and communication between components, supported by a user-friendly interface that allows operators to monitor and adjust system parameters dynamically.

The report outlines the comprehensive design methodology, simulation results, implementation process, and performance evaluation of the prototype. Emphasis is placed on mechanical and electrical integration, motion optimization, material selection, and system scalability.

List of Variables

a	Linear acceleration of the conveyor belt (m/s^2)
z	Side length (dimension) of the conveyor belt (m)
α	Angular acceleration (rad/s^2)
b	Side length (dimension) of the conveyor belt (m)
CP	Circular pitch of the rack and pinion (mm)
h_a	Addendum (tooth height above pitch line) (mm)
h_f	Dedendum (tooth depth below pitch line) (mm)
I_{belt}	Mass moment of inertia of the conveyor belt ($kg \cdot m^2$)
$I_{product}$	Mass moment of inertia of the product ($kg \cdot m^2$)
I_{rod}	Mass moment of inertia of the rod ($kg \cdot m^2$)
I_{total}	Total mass moment of inertia ($kg \cdot m^2$)
L	Length of the rod or conveyor component (m)
M	Module (ratio of pitch diameter to number of teeth, mm)
m	Mass of the component (kg)
PCD	Pitch circle diameter of the pinion gear (mm)
r	Radius of the pulley (m)
s	Side length of the cubic product (m)
T	Total time for conveyor motion (s)
T	Torque (N·m)

t_1	Acceleration time (s)
t_2	Constant speed time (s)
v_{max}	Maximum linear velocity of the conveyor belt (m/s)
Z	Number of teeth on the pinion gear
ω	Angular velocity of the rotating table (rad/s)
a	Linear acceleration of the conveyor belt (m/s^2)

List of Abbreviations

FEA	Finite Element Analysis
SDA	Serial Data Line
SCL	Serial Clock Line
ANSYS	Analysis Systems (Software)
IR	Infrared
PCB	Printed Circuit Board
PVC	Polyvinyl Chloride
PLA	Polylactic Acid
MDF	Medium-Density Fibreboard
DC	Direct Current
RPM	Revolutions Per Minute
CNC	Computer Numerical Control
ABS	Acrylonitrile Butadiene Styrene
FDM	Fused Deposition Modeling
NEMA	National Electrical Manufacturers Association
Wi-Fi	Wireless Fidelity
I2C	Inter-Integrated Circuit (Communication Protocol)
FPS	Frames Per Second
AI	Artificial Intelligence
LED	Light-Emitting Diode
CAD	Computer-Aided Design
CATIA	Computer-Aided Three-Dimensional Interactive Application (Software)

List of Equations

Equation 1: Time for Acceleration and Constant Speed (Conveyor)

$$t1 + t2 = T$$

Equation 2: Distance Calculation (Conveyor)

$$\frac{1}{2} \cdot t1 \cdot vmax + vmax \cdot t2 = Distance$$

Equation 3: Linear Acceleration (Conveyor)

$$a = \frac{vmax}{t1}$$

Equation 4: Angular Acceleration (Conveyor)

$$\alpha = \frac{a}{r}$$

Equation 5: Mass Moment of Inertia (Rod)

$$Irod = \frac{1}{12} \cdot m \cdot L2$$

Equation 6: Mass Moment of Inertia (Belt)

$$Ibelt = \frac{1}{12} \cdot m \cdot (z2 + b2)$$

Equation 7: Mass Moment of Inertia (Product)

$$Iproduct = \frac{1}{6} \cdot m \cdot s2$$

Equation 8: Total Inertia (Conveyor)

$$Iproduct + Ibelt + Irod$$

Equation 9: Torque (Conveyor)

$$T = Itotal \cdot \alpha$$

Equation 10: Angular Velocity (Rotating Table)

$$\omega = \frac{\pi}{t}$$

Equation 11: Angular Acceleration (Rotating Table)

$$\omega = \frac{\pi}{t1}$$

Equation 12: Pitch Circle Diameter (Rack & Pinion)

$$PCD = M \cdot Z$$

Equation 13: Circular Pitch (Rack & Pinion)

$$CP = \pi \cdot m$$

Equation 14: Tooth Thickness (Rack & Pinion)

$$Tooth\ Thickness = 2\pi \cdot m$$

List of Figures

List of Tables

Table of Contents

1. Introduction

Objective and Background Information:

Automated sorting systems are essential in a wide range of industries, including manufacturing, logistics, and packaging, where they enhance productivity, ensure consistent quality, and reduce manual labor and human error. As industrial processes move toward smarter and more autonomous operations, the demand for cost-effective, adaptable, and intelligent sorting solutions continues to grow. Traditional sorting systems often rely on expensive machinery or limited-function automation, making them less suitable for small-scale or customizable applications.

This project addresses these limitations by designing and implementing a low-cost, automated sorting system that integrates mechanical, electrical, and software subsystems. The system is capable of sorting objects based on shape, and visual defects, using sensor-based decision-making and closed-loop control. Key engineering objectives include developing a mechanical structure with a feeding station, conveyor belt, and rotating table optimized for precision and reliability; integrating real-time sensing components such as an ESP32 camera, load cell, and IR sensors; and coordinating these components using microcontrollers to achieve synchronized and responsive operation. Validation is carried out through Finite Element Analysis (FEA), simulations, and prototyping to ensure robustness under realistic operating conditions.

Figure 1.1: Automated Sorting System

Literature review

Background and manufacturing

- Injection Molding: Plastic granules are melted and injected into a mold under high pressure. Once cooled and solidified, the component is ejected. This highly automated process ensures high production speed and precision, as shown in figure 1.2. Regular maintenance is vital to prevent issues such as improper mold alignment, surface degradation, and residue buildup. Techniques like ultrasonic cleaning and mold release agents are used to maintain mold quality, while lubrication of hydraulic systems and inspection of heating elements ensure consistent operation. Typical defects include warping, flashing, and uneven cooling, with an error rate of approximately 1–3% (SyBridge Technologies, 2024).

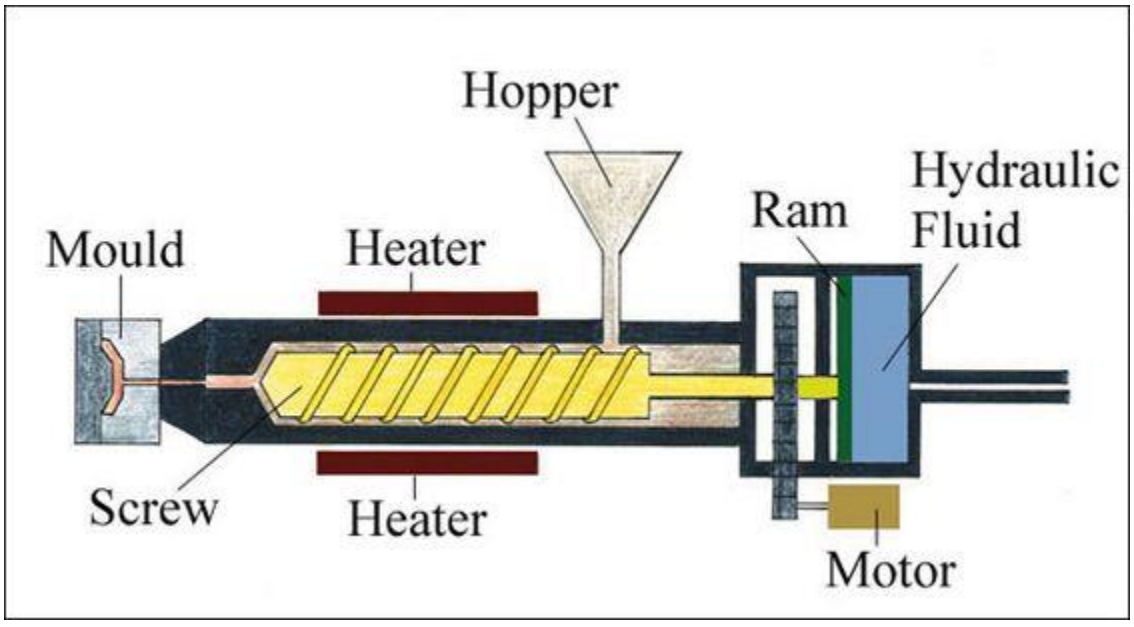

Figure 1.2: Injection Molding Process

- Die Cutting: Shown in figure 1.3, die cutting is used to produce precise shapes from materials like cardboard and foam, particularly in puzzle and packaging production. A die shaped in the desired pattern is pressed onto the material to create accurate cuts. Depending on the application, the die may be made from steel or other materials. Maintenance is crucial to prevent issues such as misalignment, rough edges, or incorrect cuts due to dull dies. This includes cleaning residue from the die, resharpening on schedule, and calibrating the system to maintain alignment. The typical error rate for die cutting is around 2–5% (Wilson Manufacturing, 2021).

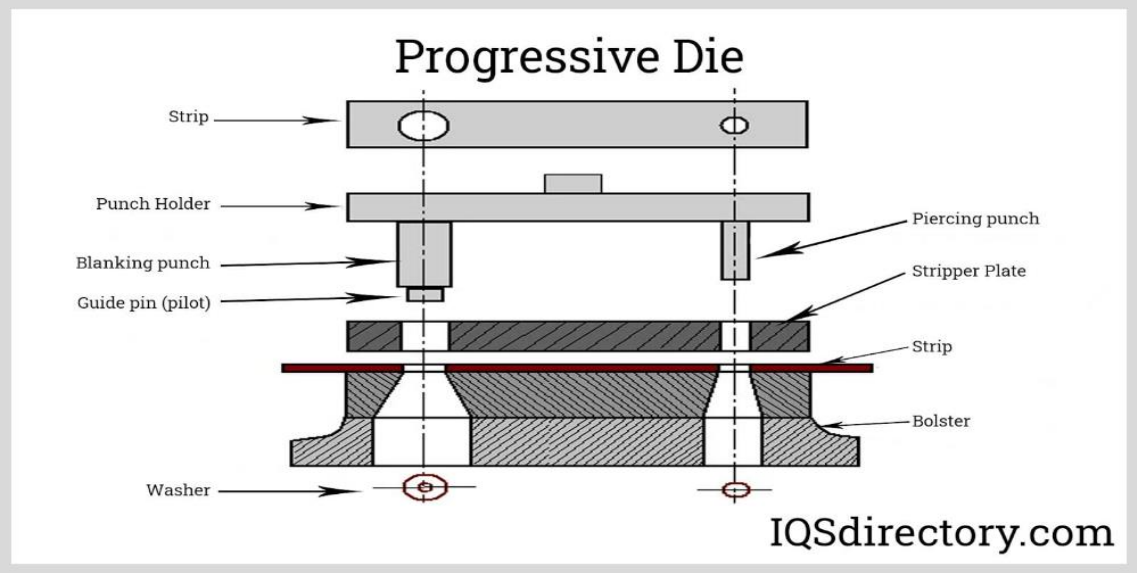

Figure 1.3: Die Cutting Process

- Rotational Molding: As illustrated in figure 1.4, rotational molding is used to manufacture large hollow plastic items by heating plastic powder inside a rotating mold. Figure 1.4 illustrates the basic mechanism on how this process is performed. The mold rotates on two axes while the plastic melts and coats the interior. After cooling while still rotating, the solidified item is removed. This method ensures uniform wall thickness but can result in defects like air bubbles or warping if not properly managed. Preventative maintenance—such as checking mold seams and heating elements, lubricating rotating parts, and cleaning molds—is key to minimizing errors, which typically range from 3–7% (Chem-Trend, 2023).

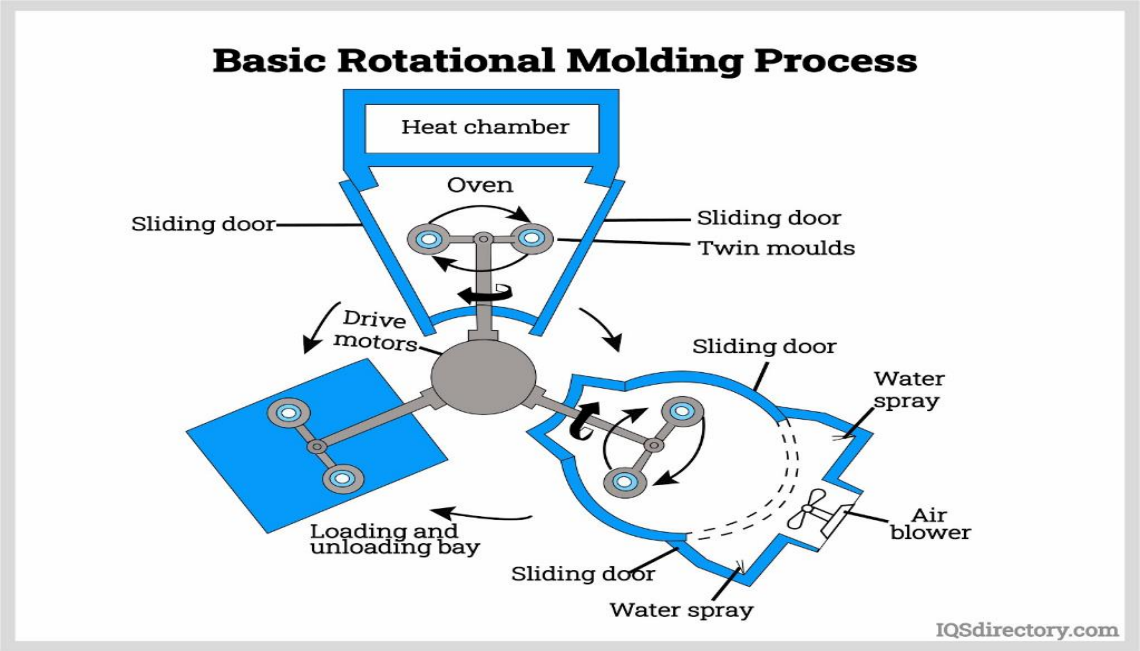

Figure 1.4: Rotational Molding Process

- Blow Molding: Blow molding creates hollow plastic parts such as containers and bottles. Heated plastic is formed into a parison and placed in a mold, where compressed air expands it to fit the mold's shape. After cooling, the final part is ejected, trimmed, and finished, as shown in figure 1.5. The process can suffer from inconsistent wall thickness, leaks, and uneven inflation if air pressure or nozzles are not properly maintained. Routine checks on air pressure systems, nozzle cleaning, and cooling system maintenance are essential. The typical error rate is around 2–6% (Wang, 2024).

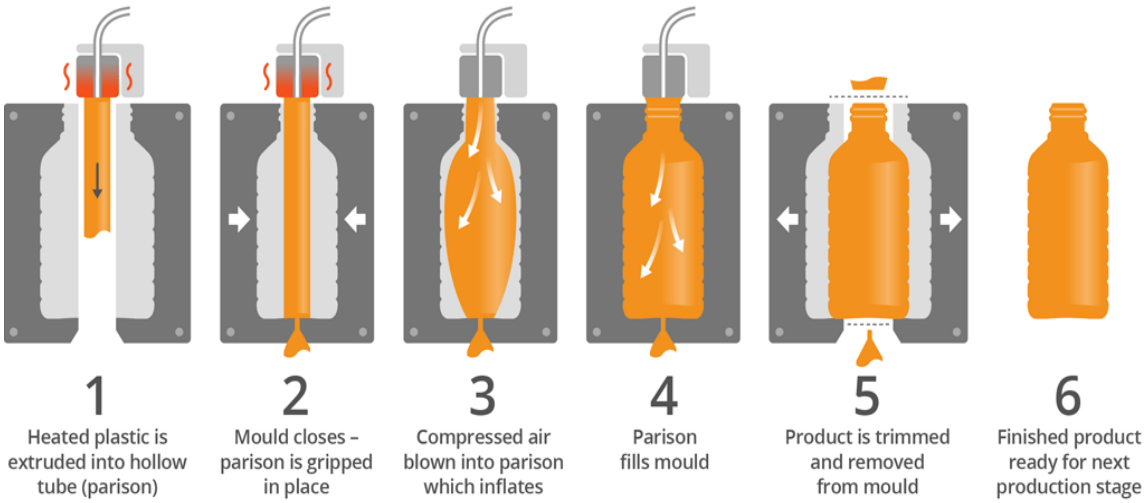

Figure 1.5: Blow Molding Process

- Woodworking: With only one of many methods shown in figure 1.6, woodworking involves shaping and finishing wood to produce toys like puzzles and blocks. Processes include cutting with saws or CNC routers, sanding, and applying finishes such as non-toxic paint. Common issues include splintering, rough edges, and incorrect dimensions, with an error rate of 3–8%. These can be mitigated by sharpening blades, cleaning sawdust from machinery, and lubricating moving parts. Maintaining sharp tools and clean equipment ensures safety and product quality (Woodworking Network, 2021).

Figure 1.6: Woodworking Process

Sorting Techniques in Industrial Automation

Sorting mechanisms are integral to modern production lines, ensuring items are categorized efficiently based on shape, size, weight, or defects.

- One prominent method is the rotating table, which uses a motorized circular platform to direct objects into different bins or paths. Its ability to rotate on multiple axes supports high-precision sorting. This system can be synchronized with sensors for accurate feedback and enhanced control. Additionally, rotating tables are efficient in multi-axis operations and CNC-based environments. However, they often require more floor space and may face inconsistent speed control due to friction or uneven loading (Automation.com, 2022).

- The suction cup gripper utilizes vacuum pressure to lift and move objects with smooth surfaces. It is durable and can adapt to various materials, making it ideal for repetitive pick-and-place tasks in packaging or electronics. Despite these benefits, suction systems may leave marks on sensitive surfaces and struggle to lift objects with sharp edges or uneven contours, as they cannot form airtight seals effectively (Piab, 2023).

- Robotic arm grippers offer high precision and adaptability, capable of manipulating objects of different shapes using specialized end-effectors. These grippers reduce sorting errors and can be tailored to specific use cases. Nonetheless, no single gripper can handle all object types, necessitating tool changes. Additionally, complex kinematics slow down processing time, reducing overall throughput (ABB Robotics, 2022).

- Pneumatic pushers mounted on conveyor belts provide fast, efficient sorting of lightweight items by using compressed air to shift objects into designated bins. These systems experience minimal mechanical wear and require low maintenance. However, air compressibility can cause speed instability under varying loads, and low-speed control is less stable compared to hydraulic cylinders (SMC Corporation, 2023).

- Bidirectional rollers offer flexible material handling by enabling movement in two directions. They increase efficiency by reversing item flow without additional conveyor infrastructure and use less energy compared to multi-motor systems. On the downside, they involve a high initial cost, require precise motor synchronization, and are subject to faster wear due to frequent directional changes (Interroll, 2022).

Object Detection in Automated Sorting Systems

Effective object detection is essential in automated sorting systems to ensure accurate classification, defect detection, and positioning. Several sensing methods can be used to identify product characteristics and defects based on various physical parameters such as color, shape, weight, and height. One possible technique is the color sensor, which can identify color inconsistencies or defects on a product's surface. This method is often used in quality control applications where visual color deviations indicate imperfections (Tarnowski & Strumiłło, 2017). However, while useful, it may not be sufficient for complex shape or structural defect detection.

Another commonly used sensor is the IR sensor, which detects the presence of an object on the conveyor belt. When the object passes in front of the sensor, it triggers actions such as halting the conveyor belt—to allow time for further inspection or scanning. IR sensors offer high-speed response and are relatively unaffected by ambient light, making them suitable for real-time detection (Rajput et al., 2020). Visual detection using cameras is among the most accurate and efficient methods for detecting shape-related defects. By integrating a camera with machine learning software such as Edge Impulse, the system can identify deformities, surface cracks, or incorrect shapes based on trained models. This technique is particularly effective when paired with real-time image processing capabilities, enabling high-throughput inspection in manufacturing lines (Pekel et al., 2022). The load cell functions as a weight sensor, distinguishing different shapes based on their mass. Defective items often weigh less or more than standard products due to missing or excess material. When integrated with a microcontroller and amplifier (e.g., HX711), load cells provide accurate weight data that can be used to confirm or reject a product (Singh et al., 2018). Although ultrasonic sensors can theoretically detect shape based on object height by measuring time-of-flight sound waves, they are susceptible to interference from nearby surfaces or structures. In enclosed guide systems, such reflections cause disturbances that degrade

accuracy. Therefore, ultrasonic sensors are less ideal for precise positioning in this context. As a result, the chosen setup for this system utilizes a camera to detect visual defects related to shape, a load cell to measure weight discrepancies as an additional defect indicator, and an IR sensor to detect the object's presence and position for pausing the conveyor at the right time. This combination offers both precision and speed while minimizing the chances of false detection due to environmental disturbances.

Control System

The control system of the automated sorting mechanism is divided into two primary layers: low-level control and high-level control, each playing a vital role in achieving precision and reliability in operation. Low-level control refers to the direct, real-time management of hardware components such as sensors and actuators with minimal processing or decision-making logic. This includes components like the IR sensor which detects the presence of objects on the conveyor. For instance, when an object arrives at the inspection area, the IR sensor immediately triggers the conveyor to halt, ensuring the object is correctly positioned for scanning. Stepper motors manage the conveyor's motion through pre-programmed steps, precisely controlling its start, stop, and speed. In addition, servo motors are used to rotate the sorting table to fixed angles—typically 0°, 120°, or 240°—according to incoming signals, allowing objects to be directed to their appropriate slots.

On the other hand, high-level control involves complex decision-making based on aggregated sensor data and intelligent algorithms. A central component in this layer is the ESP32 camera, which, when paired with a machine learning model trained on Edge Impulse, visually inspects each object. The camera can classify shapes such as cubes and pyramids and also detect surface deformities that indicate product defects. These visual insights are processed alongside input from the microcontroller, which acts as the system's brain by collecting data from the IR sensor, load cell, and camera. The microcontroller evaluates whether an object passes all required checks—shape integrity, weight tolerance, and positioning—and then decides on how to route it. For example, if the object is found to have visual defects and its weight falls outside the expected range, it is automatically directed to the reject slot.

This dual-layer control system works in tandem. Low-level control handles immediate hardware responses: the IR sensor detects an object and stops the conveyor, the load cell captures the weight, and

the motors perform physical movements like rotating the sorting table. Meanwhile, high-level control makes informed decisions based on a combination of visual and physical data, ensuring accurate sorting. Once the microcontroller confirms the object's classification, it sends appropriate commands to actuators—such as rotating the servo motor to a specific angle—thereby enabling the final sorting action.

Gantt Chart

As per Figure 1.7, the provided Gantt chart illustrates the timeline of a project, outlining four distinct processes across three quarters of a year. The initial phase, Planning & Research, is scheduled to commence in the first week of Quarter 1 and spans approximately three weeks, concluding around the end of the third week of the same quarter. Following this, the Design Process is set to begin in the fourth week of Quarter 1 and extends for roughly five weeks, reaching its completion around the eighth week of Quarter 2. Subsequently, the Simulation phase is planned to start in the sixth week of Quarter 2 and last for about four weeks, finishing around the ninth week of Quarter 2. Finally, the Integration & Assembly stage is depicted as starting in the ninth week of Quarter 2 and continuing into the third quarter, with an estimated duration of approximately five weeks, concluding around the first week of Quarter 3.

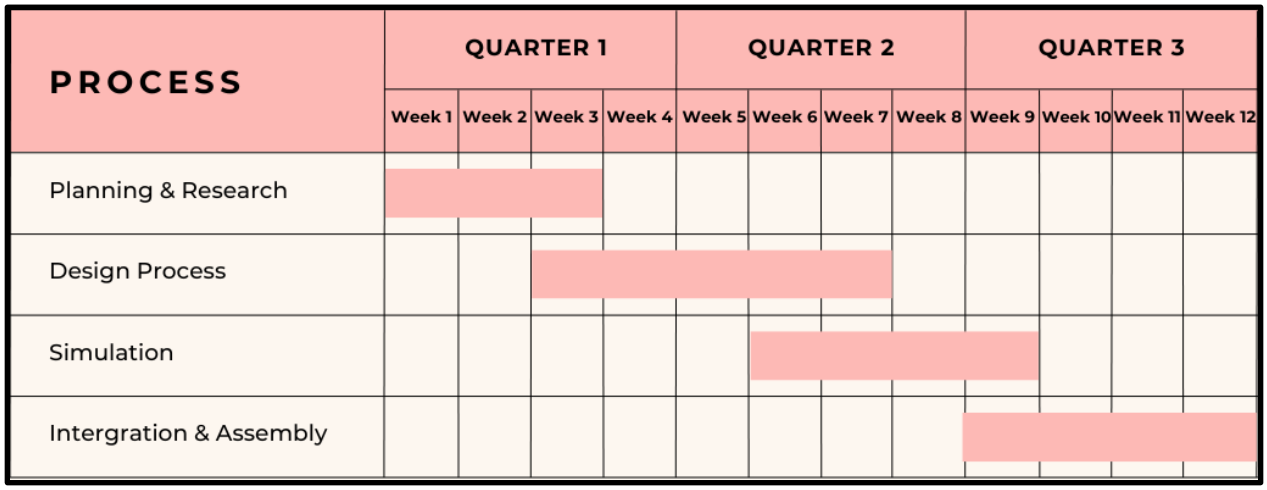

Figure 1.7: Gantt Chart

Methodology

Components

Feeding:

Rack

Pinion

LCD I2C (Helps for user interface)

Slider

I2C 16x2 Arduino LCD Screen

DC Motor (DCM-27127600-186K)

Motor Driver Module H Bridge L298 for DC motor

Kcd4 on and off switch

Emergency Shutdown Switch

Conveyor Belt

Stepper Motor: Controls the pulleys to move the conveyor belt

Motor drive drv8825 for the stepper motor

A mechanical coupler transfers torque from the motor shaft to the roller while

Compensating for minor misalignment or axial/radial displacement.

Primary and secondary rollers

Horizontal flange mounted Bearing to help reduce friction

LEDs

Sensors:

ESP-32 Cam Module

IR Sensor (E18-D80NK)

IR Sensor Module: LM393

Rotating Table:

Omnidirectional roller

Servo Motors

Sensor Selection

LM393 IR sensor

The LM393 IR sensor module was selected for object detection due to its reliability, ease of integration, and low power consumption. This module operates using an infrared emitter and receiver pair, with a typical detection range of 2–30 cm, adjustable via an onboard potentiometer. It uses a dual comparator (LM393) for stable digital output, making it compatible with most microcontrollers. The sensor is highly responsive to changes in distance and works effectively in ambient lighting conditions. Its compact size, low cost, and real-time detection capability make it ideal for applications like line following, obstacle detection, and automated positioning systems.

Infrared Sensor (E18-D80NK)

The E18-D80NK sensor is an infrared (IR) proximity sensor designed for non-contact object detection in applications such as robotics, industrial automation, and conveyor systems. It operates by emitting infrared light and detecting the reflected signal, allowing it to sense objects within a range of 3 cm to 80 cm, which can be manually adjusted (Garcia & Patel, 2021). The sensor functions on a 5V DC power supply and has a low current consumption of approximately 10mA, making it suitable for energy-efficient designs (Smith, 2020). It is commonly used in robotics for obstacle detection, conveyor belt systems for automated product sorting, and security systems for motion sensing. With its adjustable detection range, fast response time, and reliable performance, the E18-D80NK is an essential component in many automated systems. This type of sensor would be used to detect the position of the product on the conveyor belt. IR sensor used instead of passive infrared sensor, because PIR only detects infrared radiation (heat) and does not emit infrared radiation so it won’t detect the product

ESP32-CAM Module:

A camera is needed for the production line because it will detect the shape of the product and act as quality control by detecting any deformities in the shapes A ESP32-CAM module is a low-power, Wi-Fi-enabled camera module designed for applications such as video surveillance, facial recognition, remote monitoring, and industrial automation. It is powered by the ESP32 microcontroller, which provides both Wi-Fi and Bluetooth connectivity, making it ideal for wireless image transmission (Garcia & Patel, 2021). The ESP32- CAM operates within a voltage range of 3.3V to 5V and typically consumes 80mA to 310mA, depending on the processing load and Wi-Fi activity (Smith, 2020). It is widely used in security systems for real-time monitoring, automated object detection in industrial conveyor systems, smart agriculture for crop surveillance, and home automation for smart doorbells and pet monitoring. Additionally, it is integrated into AI-powered applications such as facial recognition and license plate detection. The ESP32-CAM uses an OV2640 camera module that provides the images. ESP32-CAM is lightweight, cheaper, smaller in size, and has low power consumption when compared to Kinect camera

Actuator Sizing

Conveyor

- Max speed 50 rpm = 0.0785 m/s
- Time taken = 7 seconds
- Distance = 0.5 meters
- Acceleration and constant speed

Calculating Time for Acceleration and Constant Speed

- $t1 + t2 = 8$ (where t1 is acceleration time and t2 is constant speed time)
- $(1/2) * t1 * 0.0785 + 0.0785 * t2 = 0.5$ meters
- $0.03925 * t1 = 0.0495$
- $t1 = 1.26$
- $a = 0.0623$ m/s²

- $\alpha = 4.15\ rad/s^2$

Calculating Mass Moment of Inertia (I)

- I of rod = $(1/12) * m * L^2 = (1/12) * ((\pi * 0.015^2 * 0.16) + *(\pi*0.004\text{^}2*0.1)) *1140* 0.26^2 = 7.56 \times 10^{-4} kg\ m^2$
- I of belt = $(1/12) * m * (a^2 + b^2) = (1/12) * (0.002 * 0.015 * 1.2) * 1380 * (1.2^2 + 0.015^2)$
  $= 5.96 \times 10^{-3}\ kg\ m^2$
- I of product = $(1/6) * m * s^2 = (1/6) * (0.03^3) * 1250 * 0.04^2 = 2.13 \times 10^{-5} kg\ m^2$

Calculating Total Mass Moment of Inertia (It)

- $It = 7.4933 \times 10^{-3}\ kg\ m^2$

Calculating Torque (T)

- $T = I * \alpha = 7.4933 \times 10^{-3} * 4.15 = 0.031$ Kg m = 0.31 Nm
- Nema 17 stepper have 0.35 Nm max torque

Rotating table

- rotation = π
- time = 1 second
- time of acceleration = 0.33 s
- time of constant speed = 0.33 s
- time of deceleration = 0.33 s

Calculating Time for Acceleration and Constant Speed

- $((0.33+1)/2)\times\omega = \pi$
- ω=4.72 rad/s
- α=14.3 rad/s2

Calculating Mass Moment of Inertia (I)

- I of table = mr^2 =($(\pi\times0.0152\times0.005)\times750\times(0.015)2)=1.49\times10-3$ kgm^2
- I of product = $2.13\times10-5$ kgm^2

Calculating Total Mass Moment of Inertia (It)

- I□ = $1.51\times10-3$ kgm^2

Calculating Torque (T)

- **T =** 0.022 kg m=0.212 Nm=2.2 kg cm
- MG996R Servo have an operating torque of 9.4 kg cm

Materials:

Material Selection

Feeding Station:

Body: MDF

Rack and Pinion: PLA

DC Motor Housing: PLA

Conveyor Belt:

Body: MDF

Stepper Housing: PLA

Rollers: Nylon

Body: MDF

Rotating Table:

Servo Housing: PLA

Body: MDF

Materials Description:

PVC:

PVC (Polyvinyl Chloride) was chosen as the conveyor belt material in this project due to its durability, chemical resistance, and cost-effectiveness. With a typical density of around 1.3–1.45 g/cm³ and tensile strength ranging from 25 to 60 MPa, PVC offers sufficient mechanical strength for moderate-load applications while maintaining a relatively lightweight profile. It is highly resistant to moisture, oils, and various chemicals, making it ideal for industrial environments where cleanliness and chemical exposure are concerns. PVC belts are also easier to weld, join, and clean, which simplifies installation and maintenance. Furthermore, their low surface friction helps reduce energy consumption by minimizing resistance during belt motion. In comparison, rubber is known for its excellent flexibility, shock absorption, and grip, with tensile strengths often ranging from 10 to 25 MPa depending on the type. While rubber performs well in high-impact and heavy-duty applications, it is generally heavier and more expensive than PVC, with a typical density of about 1.5 g/cm³ or higher. Rubber belts can also degrade faster in oily or chemically aggressive environments unless specially treated. For our specific use case—moderate loads, dry to mildly moist conditions, and a focus on ease of handling and cost—PVC provided a better balance of performance, durability, and affordability, making it the preferred choice over rubber.

MDF:

MDF was selected for physical construction elements such as casings and support structures due to its machinability, uniform texture, and cost efficiency. As a composite material made from wood fibers compressed with resin, MDF typically has a density between 700–850 kg/m³, which provides decent structural stability for light- to moderate-load applications. MDF typically has a Young's Modulus between 2.5 and 4 GPa and a Poisson's Ratio of about 0.25 to 0.35. These values give MDF moderate stiffness and limited elasticity. Its relatively low Poisson's ratio means it doesn't deform much laterally, helping it maintain dimensional stability Its consistent internal structure allows for clean, accurate cuts and drilling without splintering, making it suitable for precision work. In our case, MDF was used for components where high moisture resistance or flexibility was not necessary, such as dry

indoor environments. It also provides excellent adhesion for paint and veneer finishes, adding to its versatility.

When comparing materials, both acrylic and aluminum were evaluated. Acrylic offered high visual clarity and a respectable tensile strength of around 70 MPa, but its cost and brittleness during machining made it less suitable for our needs. Aluminum, by contrast, offered superior mechanical strength (typically 90–300 MPa depending on alloy) and excellent corrosion resistance. However, its higher density, about 2.7 g/cm³, made it considerably heavier than both MDF and acrylic, which was a disadvantage for applications where weight reduction was desirable. Additionally, aluminum required specialized cutting tools and introduced more complexity and cost to the fabrication process. Since our application did not demand high mechanical strength or thermal conductivity, MDF provided the most practical and efficient solution. Its low cost, ease of shaping, and sufficient structural integrity made it the ideal material choice for this project's construction components.

PLA:

PLA was chosen for 3D printing in this project due to its reliable performance and compatibility with standard FDM setups. While PLA typically prints well without a heated bed, we used one set to around 60°C to ensure stronger adhesion and minimize warping, particularly for larger or longer prints. PLA provided a good balance between strength and ease of printing, offering a tensile strength of approximately 50–70 MPa and a density of about 1.24 g/cm³ and a Young's modulus 2.7–16 GPa., and a Poisson's Ratio of about **0.33 to 0.36**. Its higher modulus, especially in more crystalline or industrial-grade forms, makes PLA a stiff material, ideal for parts that need to hold their shape. However, it also tends to be brittle, as the material doesn't flex much before breaking. The moderate Poisson's ratio indicates limited lateral deformation, which contributes to its rigidity but reduces its impact resistance. which made it ideal for producing rigid structural housings and support components that didn't require high flexibility or impact resistance. Its dimensional accuracy was consistent, and the parts had a clean surface finish with minimal post-processing required. The material's glass transition temperature, around 60°C, and its relatively low melting point of 180–220°C allowed for efficient printing using basic extrusion systems. While not suited for high-heat environments, PLA's rigidity and shape retention made it a great fit for enclosures, fixtures, and static mechanical parts in our setup. Additionally, compared to alternatives like ABS, PLA required lower printing temperatures, produced fewer fumes, and resulted in a cleaner and simpler printing process.

Nylon 6:

MDF was selected for structural parts of the project due to its ease of machining, smooth surface, and affordability. It is an engineered wood product formed from compressed wood fibers and resin, offering a consistent texture and uniform density. Its ability to be cut, drilled, and shaped easily makes it ideal for applications requiring precise geometry and clean finishes. MDF is especially suitable for non-load-bearing components, casings, and enclosures in dry environments. Although it is not as strong or moisture-resistant as solid wood or certain plastics, it provides an excellent surface for painting and laminating. **Nylon 6** has a Young's Modulus ranging from **2.0 to 3.2 GPa** and a Poisson's Ratio between 0.35 and 0.45. This combination gives Nylon a good balance of stiffness and flexibility. The moderate modulus allows it to withstand loads without being overly rigid, while the relatively high Poisson's ratio means it can undergo significant lateral deformation when stretched. These properties make Nylon 6 suitable for durable, load-bearing applications where toughness and resistance to wear are important. Compared to acrylic, MDF was chosen due to significant cost savings. Acrylic, while offering transparency and higher impact resistance, is more expensive and prone to cracking under machining stress. Since transparency and high-end aesthetics were not required, MDF was the more practical option, offering both sufficient strength and easier fabrication within a limited budget.

Conceptual Design

Suction Cup:

The design incorporates a suction cup mechanism powered by a vacuum source, which generates the negative pressure required to securely hold various objects. An adjustable seat, threaded into the body, allows for fine-tuning of both suction strength and positioning, offering precise control. Within this seat lies a spring, housed in a cavity, which provides controlled movement and flexibility during operation. A spherical poppet regulates airflow and facilitates vacuum release when necessary. To maintain system integrity, a filter is included to prevent dust and debris from entering the mechanism. The centering rest ensures that the suction cup is correctly aligned, while the cup fitting connects the cup to the main system. The suction cup itself forms a vacuum seal to grip objects securely, and the airflow path is designed to allow for both efficient suction and quick release. This mechanism is illustrated in figure 2.1.

Integrated into a robotic arm mechanism, the system enables precise and flexible movements, enhancing its utility in various automation tasks. The end effector, designed as a suction cup gripper, enables the system to create a temporary vacuum for object gripping and ensures rapid detachment for operational efficiency. For handling heavier objects, a conveyor system is incorporated to ensure smoother transportation and object sorting. As shown in figure 2.2 , a concept design was made to fit this system's application

Inspired by designs such as those used in AIRBEST systems, the application scope of this mechanism includes moving components along assembly lines, transporting delicate materials like glass sheets without causing scratches, and lifting or positioning large parts such as windshields and automotive body panels.

Figure 2.1: Suction Cup Mechanism

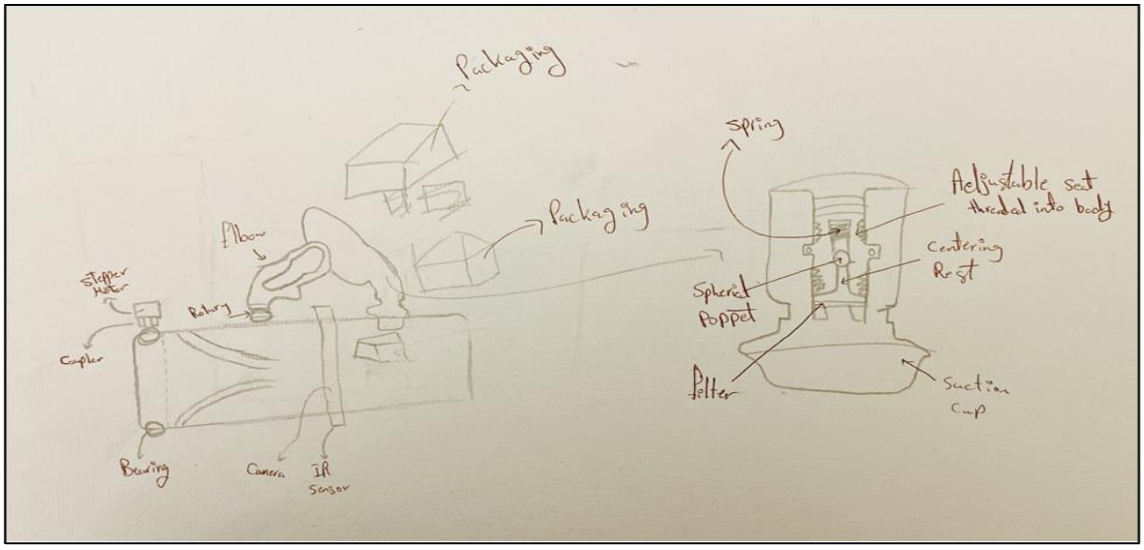

Figure 2.2: Suction Cup Concept Design

Robotic Arm Gripper

The design features a robotic arm mechanism composed of multiple joints—namely rotary, revolute, and spherical—which together provide a wide range of motion suitable for complex manipulation tasks. The arm is capable of reaching and orienting itself accurately to interact with various components on the production line. Attached to the arm is the end effector, or gripper, which includes a rotary joint to adjust the orientation of the object being handled. This mechanism securely grasps objects and transfers them efficiently to the designated packaging area. The design of this robotic manipulation system is illustrated in Figure 2.4

Complementing the robotic arm is a conveyor system driven by a stepper motor, which ensures controlled and precise movement of objects along the line. Components such as bearings and couplers contribute to the smooth, vibration-free operation of the belt. As objects progress along the conveyor, they are identified and retrieved by the robotic arm for sorting. The process culminates in the packaging stage, where the robotic arm deposits sorted items into an open container, which serves as the packaging box. This packaging setup is shown in Figure 2.3

Applications of this design span several industries. In industrial automation, the system is used for sorting and packaging components along manufacturing lines. In food processing, the robotic gripper handles food items with care, ensuring proper packaging and maintaining hygiene standards. The design also finds relevance in electronics assembly, where it helps position delicate components with high precision, and in logistics and warehousing, where it streamlines the packaging of items for shipment. This concept builds upon principles outlined by Bennett Brumson (2001), highlighting its relevance and adaptability in modern automation systems.

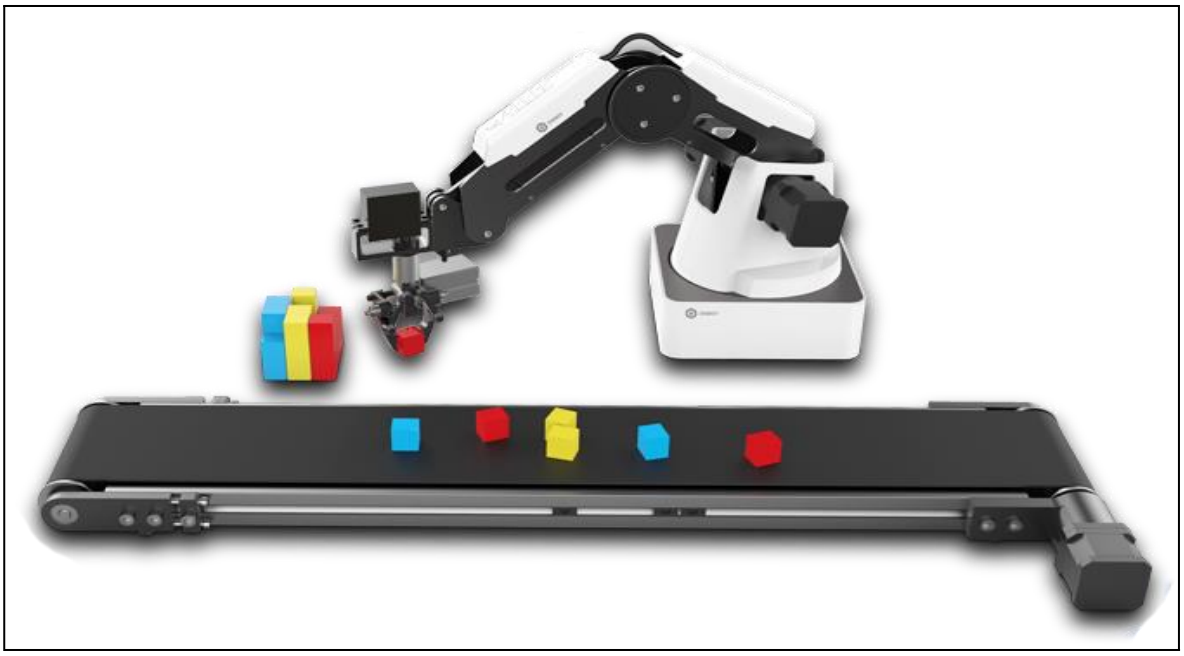

Figure 2.3: Robotic Arm Gripper Mechanism

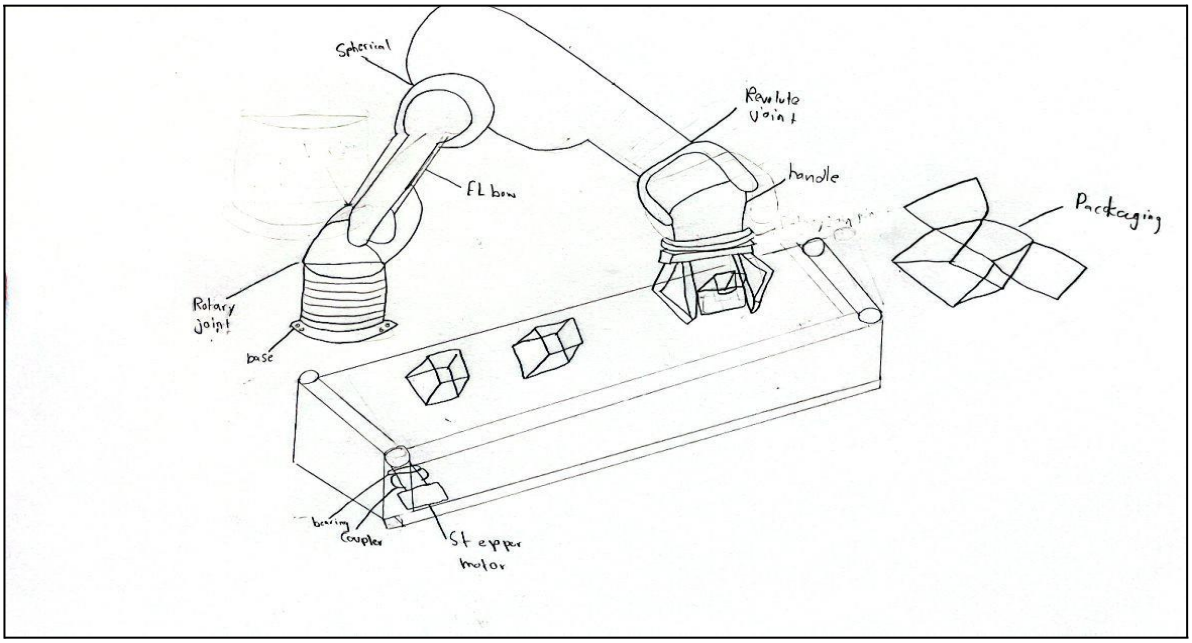

Figure 2.4: Robotic Arm Gripper Conceptual Design

Rotating Table

The design incorporates a rotating table mechanism driven by a stepper motor, which enables precise control over angular positioning. A coupler connects the motor to the shaft, transmitting torque effectively. To manage the axial load from the weight of the table, a thrust bearing is placed at the motor end, minimizing friction and ensuring smooth rotation. The cross-section of the shaft and the mating hole are specially milled to facilitate rotational motion, allowing the table to operate reliably under load. This system is demonstrated in Figure 2.5 with its conceptual design illustrated in Figure 2.6

In addition to the rotating table, a conveyor system mechanism is implemented. While it shares similarities with the rotating table in terms of motor-driven operation, it differs in that a ball bearing is used instead of a thrust bearing, as there are no significant axial forces present. The shaft is connected to the driver roller, with a secondary roller at the opposite end to support the conveyor belt movement. The final stage of the process is the packaging station, which features slots that open when a product reaches a specific position. A sloped guide is used to direct the product smoothly into its designated packaging location. The design of the packaging mechanism is shown in Figure 2.

As described by Parkson Wu (2024), this system finds broad applicability across multiple sectors. In food processing, it can sort various fruits based on size and shape. In material sorting, the mechanism efficiently separates recyclable from non-recyclable materials. Additionally, the system contributes to quality control by identifying and sorting defective products from acceptable ones, enhancing both productivity and product consistency.

Figure 2.5: Rotating Table Mechanism

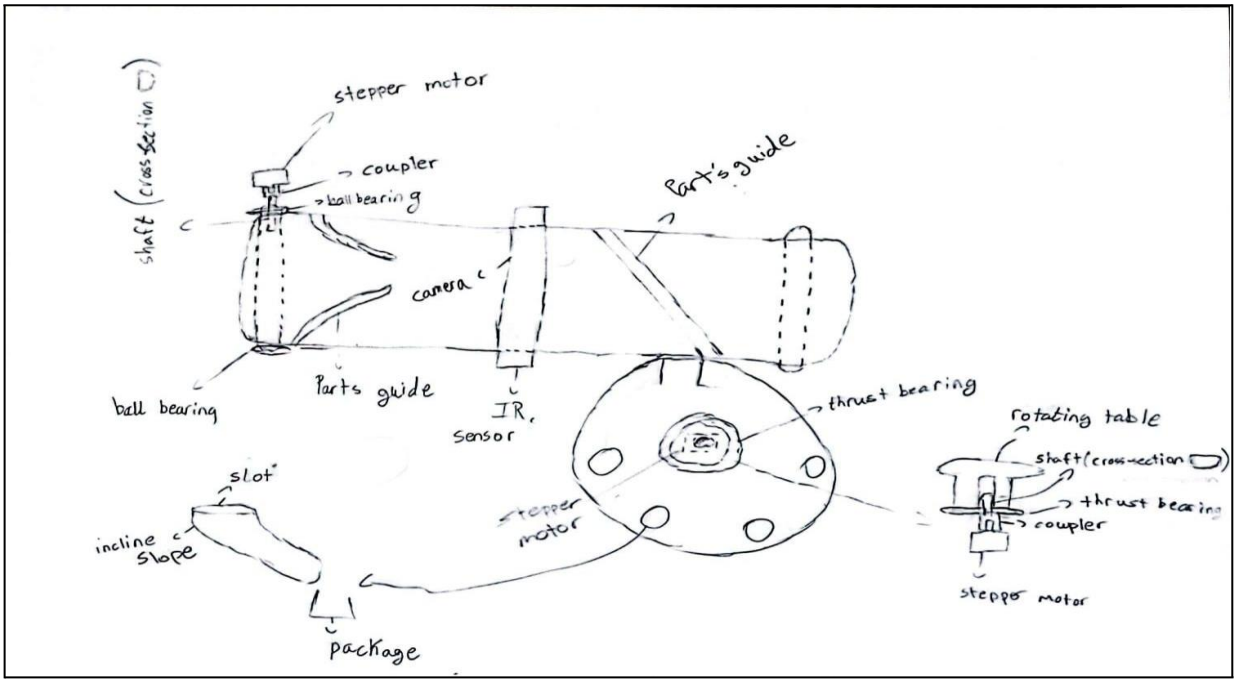

Figure 2.6: Rotating Table Mechanism

Conveyor Belt Actuators

This design features an actuator mechanism, primarily pneumatic, that serves multiple functions along the system. It is used to push defective items off the conveyor belt or redirect shaped components into designated boxes for sorting and packaging. Additionally, the actuator assists in the feeding process by pushing blocks or items onto the conveyor belt, ensuring a consistent flow of materials. The conveyor belt system operates using a NEMA stepper motor, which delivers precise motion control. A coupler connects the motor to the shaft, which is in turn linked to the driver pulley. A second support pulley wraps around the other end of the belt to maintain alignment and belt tension. To reduce rotational resistance and ensure smooth operation, ball bearings are incorporated into the system (OCS, 2019). The complete actuator and conveyor integration is depicted in Figure 2.7, with the conceptual design is shown in Figure 2.8. Applications for this system are wide-ranging. In food farms, it enables the rapid and effective removal of defective produce, streamlining post-harvest processing. Additionally, in raw material and resin handling, the system aids in consistent movement and sorting, supporting both quality control and operational efficiency.

Figure 2.7: Conveyor Belt Actuators Mechanism

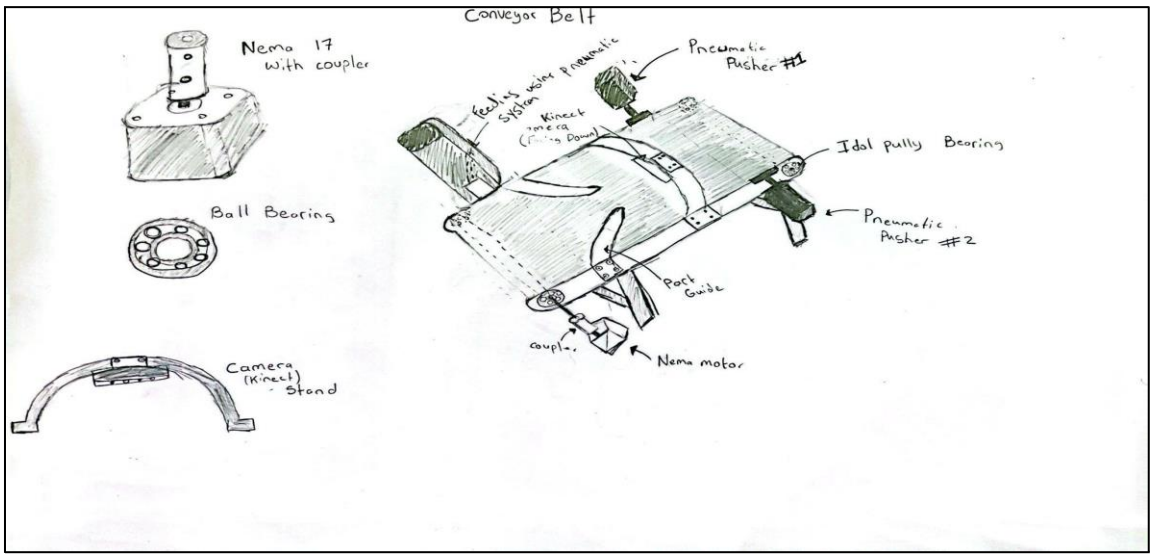

Figure 2.8: Conveyor Belt Actuator Conceptual Design

Conceptual Design Comparison

- Using a scoring-based system 1 being the lowest and 5 being the highest rating, different criteria will be used with different weights to pick the best sorting mechanism according to the scoring system. Criteria are cost, speed, ease of implementation, ease of manufacturing, and handling and care. Starting with cost, it contains a significant weight of 20% because of the category of being university students and under a budget that cannot be exceeded. Robotic arm grippers are considered the most expensive due to the complexity of mechanism and the use of multiple motors and actuators for joints and grippers. According to Kortberg(2024), Suction cup based grippers are the most cost-effective grippers without affecting efficiency or functionality. Rotating table and conveyer belt with actuators are more cost effective than grippers due to using less complex design which would lower manufacturing costs. When compared together, the actuators used would be more expensive than the motors used in a rotating table; however the rotating table would require an external body other than the conveyor belt which would lead to the similarity of costs between them getting the same rating.

- The Second Criteria is speed, since this application of sorting and handling in factories needs a higher and better overall speed to increase productivity. The Robotic Arm could be made to be fast but due to its complex structure and its need to be precise in moving. Also as well due to the gripper being able to control one item at once. Conveyor and actuator since the pneumatic system will be linear movement along the conveyor and it relies on air pressure it should be pretty quick at pushing off the product. The rotating table due to it being able to have one product at a time to sort cuts the speed a lot since it's not multiple products but it's better than the robotic arm and suction because of ease in design and structure. Suction Gripper is not the best optimum speed because of the time it will take to seal the vacuum between the product and the suction, but adding on to that the fact it only sorts one product.

- Ease of implementation is how easy a system can be processed and operating successfully.Therefore, the weight is not as high when compared to other criterias due to its low requirements. Robotic grippers are known by their complexity to program and integrate other systems precisely which would lead to receiving the lowest score. Additionally, suction cups still have the difficulties of robotic arm grippers due to implementing positional analysis of the gripper at the correct location when needed; however, suction cup grippers are simpler than arm grippers, even though there are still difficulties like handling the variation of shapes, so its rating would be the second lowest. Implementing a rotating table is moderately complex due to the mechanical setup of the table and synchronizing both conveyer and rotating table together. Furthermore, implementing the actuator is relatively complex due to timing the actuator by integrating the sensor input and tracking the belt of the conveyer. Consequently, rating of actuator and rotating table is similar.

- Ease of Manufacturing is essential due to the project having to create the parts and structure and mechanism overall together. Hence ease of manufacturing is another criteria for selecting the final concept. The Robotic Arm, due to it being moving around in different directions would need a proper structure base, mounts, with the right and precise holes. That could be more challenging when it comes to manufacturing cause a lot of little details will matter including the body. The conveyor and actuator is one of the simplest since the body would not have anything connected to it moving it around but the legs of the belt to create stability. The Rotation table has the same idea as the conveyor actuator, but to its motion being different and a lot of the body part would need proper and very detailed manufacturing to avoid unnecessary instability. The Suction Cup also its complexity makes the manufacturing part very complicated like the robotic arm because of the need of many parts and different ways to stabilize the suction.

- Handling and care is the ability of the sorting mechanism to handle the product without causing any damage to the product. Therefore, it would receive a high weight due to the purpose of the production line being quality and sorting. Robotic

arm gripper excels in this criteria due to its precision and dexterity, which could be controlled to accurate placements and reducing any risk of damage. However, suction cup grippers struggle in this criteria due to the issues when dealing with different shapes and leaving marks on the product after lifting due to the suction (Bouchard, 2024). Actuator struggles as well in this criteria due to the rough handling of pushing items of the conveyor which could lead to collisions and increase the risk of damage. Finally, rotating table excels in this criteria due to the gentle process of placing and removing item from the table; however, there is still the possibility of the product to slide during rotating, so the robotic arm gripper would be optimal in this criteria.

After Comparing and looking at all concepts we concluded the best Design and mechanism to implement and use would be the rotating table. Since it had the highest overall score of 3.65 out of 5.

Conceptual design comparison

	Weight	Robotic arm Gripper		Conveyor Actuator		Rotating Table		Suction cup gripper	
		Rating	Weighted Score	Rating	Weighted Score	Rating	Weighted Score	Rating	Weighted Score
Cost	20%	1	0.2	4	0.8	4	0.8	2	0.4
Speed	15%	2	0.3	4	0.6	3	0.45	2	0.3
Ease of implementation	20%	1	0.2	3	0.6	3	0.6	2	0.4
Ease of manufacturing	20%	2	0.4	5	1	4	0.8	3	0.6
Handling and Care	25%	5	1.25	2	0.5	4	1	2	0.5
	Total score		2.35		3.5		3.65		2.2
	Rank	4		2		1		3	
	continue	No		No		Develop		No	

Table 1.1: Conceptual Design Comparison

Manufacturing Processes

3D Printing

3D Printing is one of the modern manufacturing processes used. Its repetitive and additive process adds material layer by layer till the desired 3D shape is made. A CAD is made of the desired part and turned into a digital file to be given to the 3D printer (HuAlicia, 2025). Each layer added is the cross section at that specific part of the CAD. 3D printing can produce complicated shapes without the need of going through more complicated manufacturing processes like casting, forming, moulding, etc. The Materials that are mostly used are PLA, PLA+, Eco PLA. PLA is what will be used for the entirety of the project. It is stiff and easy to print with, but its impact, chemical, and temperature resistance are not ideal. PLA+ is just an enhanced version of PLA with higher resistances, but due to that fact it is more costly than PLA. ECO PLA is easy to use, higher quality surface finish, and it's made mostly out of recycled materials, but it’s more expensive than PLA (UltiMaker, 2025). The Printer used for the entire project is the ANYCUBIC Chiron. First Step is to make the desired 3D part using a CAD software. After that saving the file as stl (stereolithography) and opening it through a 3D printing software (Adobe, 2025). The 3D printing software to be used is UltiMaker Cura, due its recommendations through fellow colleagues and due to its easy and friendly interface. After Importing the file choosing the print settings. First step was changing the infill density to 25% to lower printing time, save material and still get a good strength. Less than that it would be for smaller products or products that won't handle any loads. Heavier than 50% is material and time consuming but the product comes out really strong (O'Connell, 2023). After picking density we choose the infill pattern there are many various patterns each with different 3 strengths but also printing times. The Patterns used will all be mostly Zigzag due to its strength and lower printing time it's the best option. The Printing Temperature was set to 220 because the pla material is between 200-225, and the build plate temperature to 70 to not allow in hardening or shrinking to allow

Laser Cutting

For fabricating the main structural components of the conveyor belt and rotating table, we used laser cutting with 5 mm MDF sheets. The process began by designing the required parts in CATIA, where we precisely modeled the main body, supports, and rotating table geometry. Once the design was finalized, we exported the drawings in .dxf format, which is compatible with most laser cutting software and machines. This format preserves the 2D geometry needed for accurate cutting paths. The 5 mm MDF was chosen for its flatness, ease of cutting, and sufficient strength for structural parts. After exporting, the .dxf files were loaded into the laser cutter software, where we configured the cutting parameters like power and speed suitable for MDF. The laser cutter then followed the outlines exactly, producing clean and accurate cuts. This method allowed for fast, repeatable, and precise fabrication of all parts, significantly reducing manual labor and ensuring all components fit together as planned during assembly.

Mechanical Design

Feeding Station

Mechanism

The rack and pinion mechanism in this project serves as the main driver for the feeding station within an automated sorting system. After the product falls through the main body, shown in figure 2.9, its function is to push individual products onto a conveyor belt for further processing. The setup includes a pinion gear shown in figure 2.12, driven by a motor mounted directly onto its shaft, and as shown in figure 2.10 a rack that converts the rotary motion into linear movement. The rack is connected to a custom-designed slider part beneath it, figure 2.11. This forms a male-female interface that guides the rack along a straight path and ensures stability during motion. As the motor turns the pinion, the rack advances within the slider, smoothly pushing products forward. This arrangement provides precise and controlled feeding, ideal for small loads between 100 and 300 grams. Both the rack and the slider components were 3D-printed to allow for easy customization, accurate fit, and cost-effective production. The result is a reliable and compact feeding solution within the larger automated system.

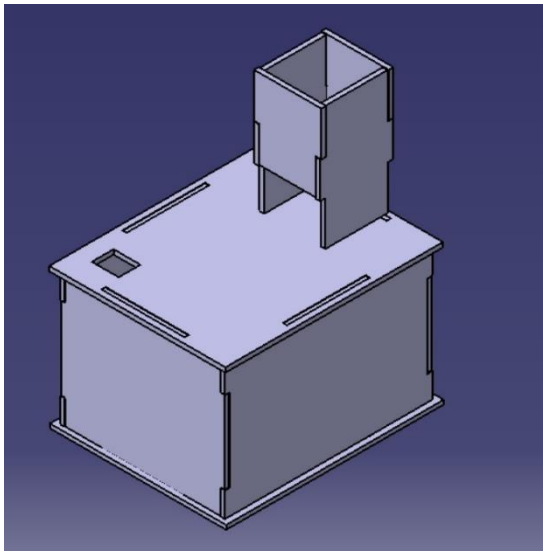

Figure 2.9: Feeding Station Main Body

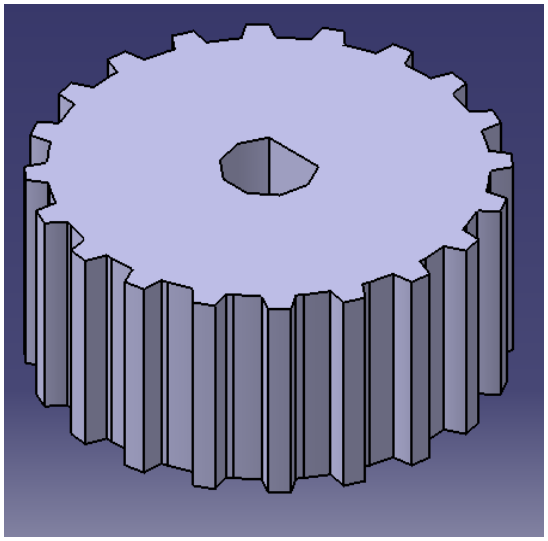

Figure 2.12: Feeding Station Pinion

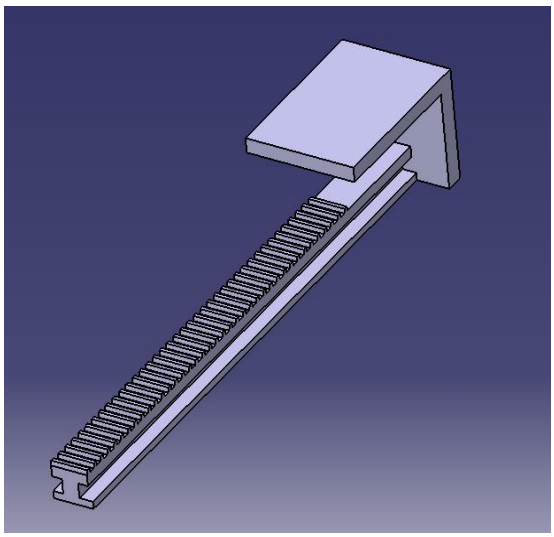

Figure 2.10: Feeding Station Rack

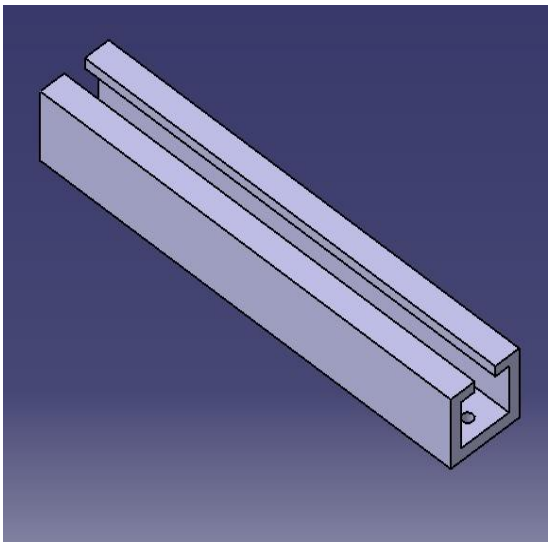

Figure 2.11: Feeding Station Slider

Rack and Pinion Calculations

Designing the rack and pinion required multiple calculations to ensure proper system functionality. The module (M), which is the ratio of the circle pitch of the gear to pi, was chosen as 1 mm. A smaller module results in finer teeth, improving precision, reducing backlash, and maintaining a compact design while providing sufficient strength for the 100g-300g load (Shigley & Mischke, 2015). The pitch circle diameter (PCD), calculated as 20 mm, defines the effective diameter where gear teeth engage; it offers a compact size while ensuring proper meshing (Norton, 2006). The outer diameter (OD), calculated as 22 mm, represents the maximum diameter of the gear and ensures the teeth are fully formed without interference or unnecessary material removal (Dudley, 1994). The circular pitch, found to be 3.14 mm, is the distance along the pitch circle between corresponding points on adjacent teeth and ensures proper spacing for rack engagement (Khurmi & Gupta, 2005). The tooth thickness of 1.57 mm represents the width of a single tooth at the pitch circle, balancing force transmission and minimizing backlash (Shigley & Mischke, 2015). The addendum (ha), set at 1 mm, is the height of the tooth above the pitch line, while the dedendum (hf), set at 1.25 mm, is the depth of the groove below the pitch line; the slightly deeper dedendum provides clearance to prevent interference (Dudley, 1994). The total tooth height of 2.25 mm ensures complete engagement between the gear and rack. On the rack side, the groove depth was matched to the dedendum for alignment, and the groove width was set to 2 mm slightly larger than the tooth thickness to reduce friction during movement (Buckingham, 1988). Finally, the rack length was chosen to be 150 mm to accommodate the application's required range of motion (

.

Parameter	Formula	Value	Units
PCD	PCD = m × Z	20	mm
CP	OD = (Z + 2) × m	22	mm
Tooth Thickness	(π × PCD) / Z	3.14	mm
Ha	(π × m) / 2	1.57	mm
Hf	Hf= 1.25 x m	1.25	mm
Total Tooth Height	h = ha + hf	2.25	mm
Groove Depth	----------	2.25	mm
Groove Width	----------	1.25	mm
Rack Length	----------	150	mm

Conveyor Belt

The conveyor belt subsystem is responsible for transporting products through the sorting process and is supported by nylon rollers on each side, which provide smooth and stable motion. As the product moves along the belt, it first passes an IR proximity sensor that detects its presence. This triggers the stepper motor to pause the conveyor, allowing the ESP32-CAM module to capture an image of the product. The module processes the image to classify the item as a pyramid, cube, defective pyramid, or defective cube. A part guide is positioned to help align the product toward the center of the conveyor belt before image capture, reducing classification errors by the camera. The stepper motor drives the conveyor belt via a drive pulley, which is coupled to the motor shaft using a mechanical coupler. Both the drive and driven pulleys incorporate flange ball bearings on their shafts to reduce friction and wear, enabling smoother and more efficient rotation. Once classification is complete, the conveyor resumes motion. At the end of the belt, a stick-like deflector gently diverts the product toward a side gap in the conveyor, allowing it to drop through the opening onto a rotating table positioned below. Additionally, the conveyor belt frame features specially designed slots and grooves that allow for adjustable tensioning. By loosening fasteners, the housed bearing shaft positions can be shifted along the slots to either tighten or loosen the belt. This feature ensures proper alignment, reduces slippage, and extends the system's lifespan by maintaining optimal belt tension during operation

Body

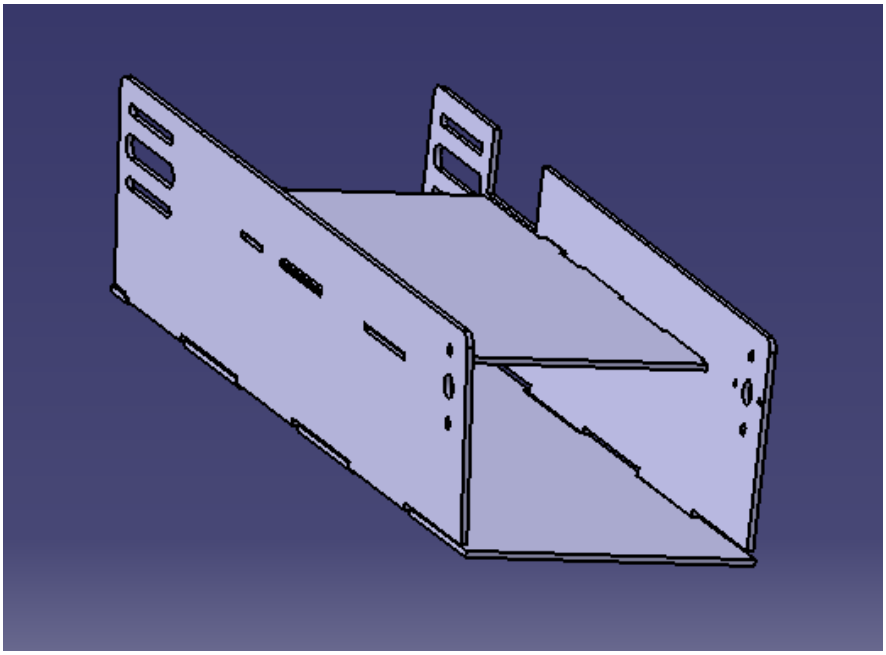

Figure 2.13: Conveyor Belt Body

Rotating Table

Rotating table Final Design to be put together to complete the last and final stage, shown in figure 2.17. Its job is to rotate the servo motor depending on the selected criteria chosen by us through the camera. The servo is to rotate the top base of the rotating table to one of the two slots shown in figure 2.14 one being for the qualified shapes and one being for the defected shapes. Once rotated the servo gates attached to the bottom will open depending on which slot the sensors send it to. Figure 2.15 is the layer of the table that will be attached to a servo motor to control angle to where to send the product, the holes on top are to mechanically fasten the table to the motor. Figure 2.16 shows the bottom layer where the rotating table puzzle will fit

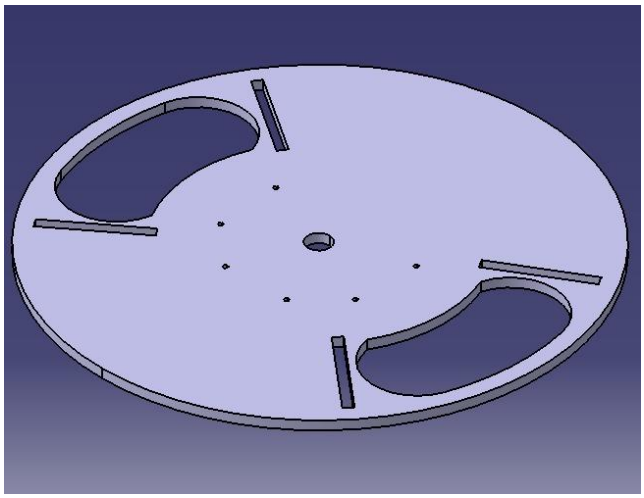

Figure 2.14: Rotating Table Slots Layer

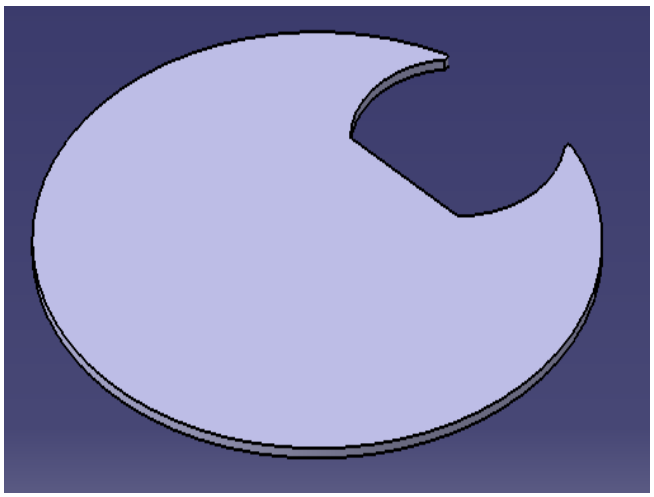

Figure 2.15: Rotating Table Moving Layer

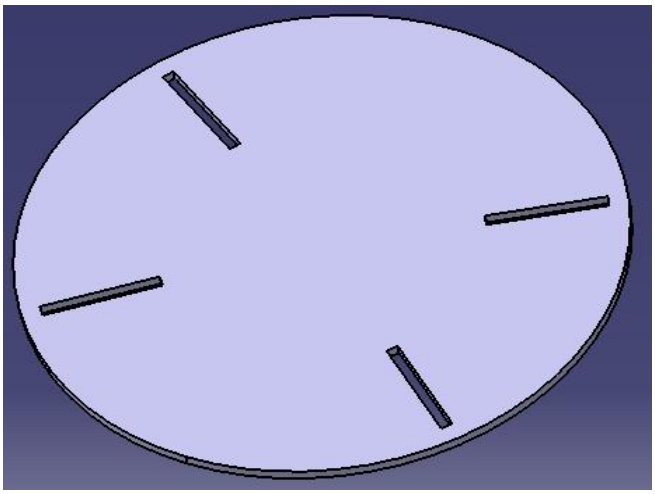

Figure 2.16: Rotating Table Bottom Layer

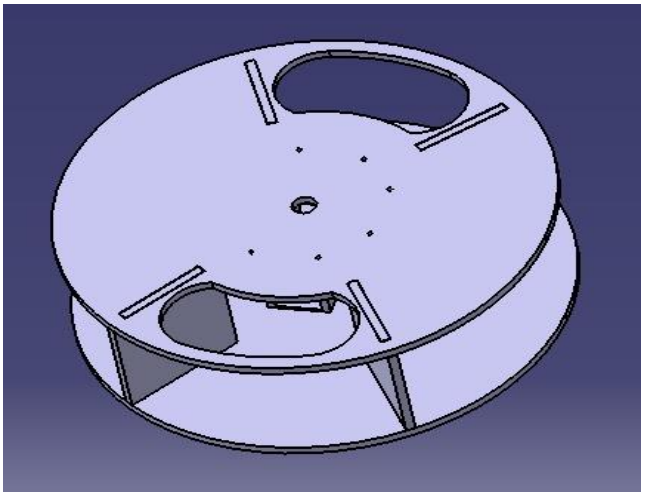

Figure 2.17: Rotating Table Assembly

Stress Analysis

Rollers

A static structural analysis was performed using ANSYS 2024 R2 to evaluate both the total deformation and equivalent (von Mises) stress distribution in a cylindrical roller subjected to a torsional load. The model consists of a central cylindrical roller with extended shafts on both ends. A moment was applied at the tip of one shaft, while both ends were constrained using cylindrical supports to allow rotation but restrict linear displacement.

The total deformation results, as shown in Figure 1, indicate a maximum displacement of approximately 0.0728 mm near the free end where the moment was applied. The deformation gradually decreases toward the opposite end, where the cylindrical supports are applied, reaching a minimum of 0 mm. This deformation pattern is consistent with torsional loading, where twisting occurs about the longitudinal axis of the roller. The smooth distribution of displacement across the roller body confirms that the structure is undergoing a typical elastic twist, with no signs of discontinuities or irregular deformation.

The equivalent (von Mises) stress results, as shown in Figure 2, reveal a maximum stress of approximately 2.9915 MPa, occurring near the region where the moment is applied. The stress decreases progressively along the roller body and becomes minimal near the fully constrained end. This stress distribution is also characteristic of torsional loading, where the highest shear stresses occur at the outer surfaces and near the point of torque application. The minimum stress value, recorded as approximately 1.34×10^{-12} MPa, occurs in the fully supported region, indicating that the boundary conditions were effectively applied.

The combined analysis of Figures 2.18 and 2.19 demonstrates that the roller behaves elastically under the applied moment, with both stress and deformation remaining within safe limits. The von Mises stress values are significantly lower than the typical yield strength of common structural materials, suggesting that the component is not at risk of failure under the given loading conditions. The mesh used in both simulations appears sufficiently refined, with no visual signs of element distortion, supporting the accuracy of the results. Overall, the structural response under torsion is as expected, and the design can be considered safe for the applied loading scenario.

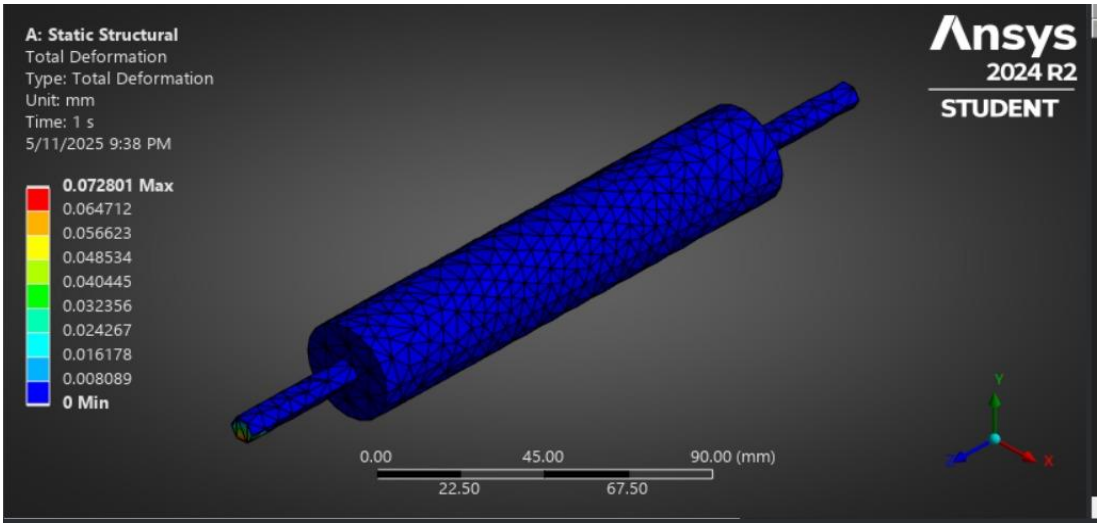

Figure 2.18: Roller Deflection in mm

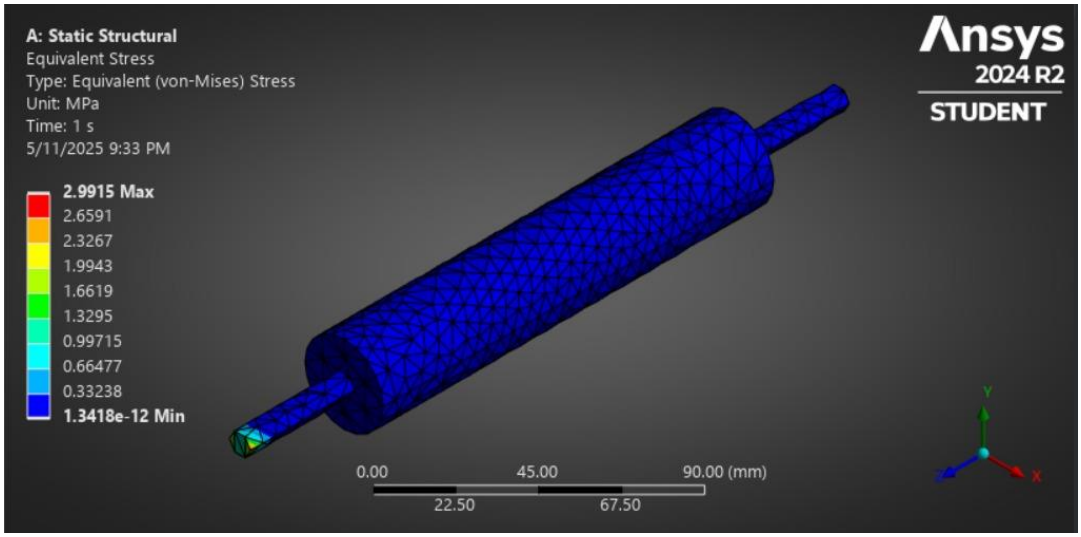

Figure 2.19: Roller Stress in MPa

Stepper Motor Housing

The static structural analysis, as depicted in Figure 1 (Equivalent Stress), reveals a maximum equivalent (von-Mises) stress of 0.28034 MPa, with stress concentrations evident around the mounting holes and the stepper motor interface. This localized high-stress region necessitates a comparison against the material's yield strength to ascertain the structural integrity and factor of safety under the applied load. Simultaneously, the total deformation analysis, illustrated in Figure 2 (Total Deformation), indicates a maximum displacement of 0.00014917 mm, observed in the areas of the housing furthest from the fixed mounting points. This minimal deformation suggests a stiff structural response to the applied loading. However, the potential impact of this small displacement on the overall system's functional requirements, particularly regarding precise alignment, warrants further consideration. A comprehensive evaluation would necessitate additional analyses, including factor of safety calculations based on material properties, fatigue assessments under operational conditions, modal analysis to identify natural frequencies, and sensitivity studies to understand the influence of variations in load and material characteristics on the structural behavior, as inferred from the presented figures.

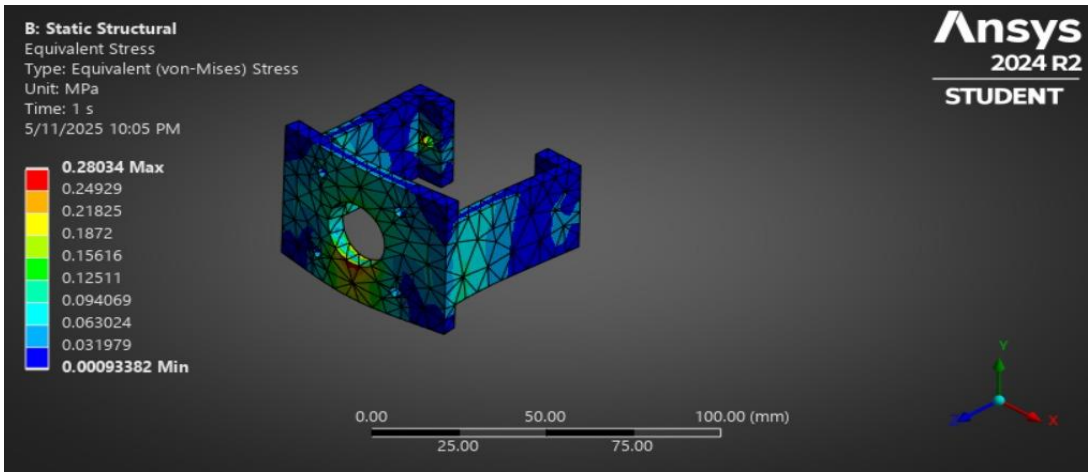

Figure 2.20: Stepper Motor Housing Stress in MPa

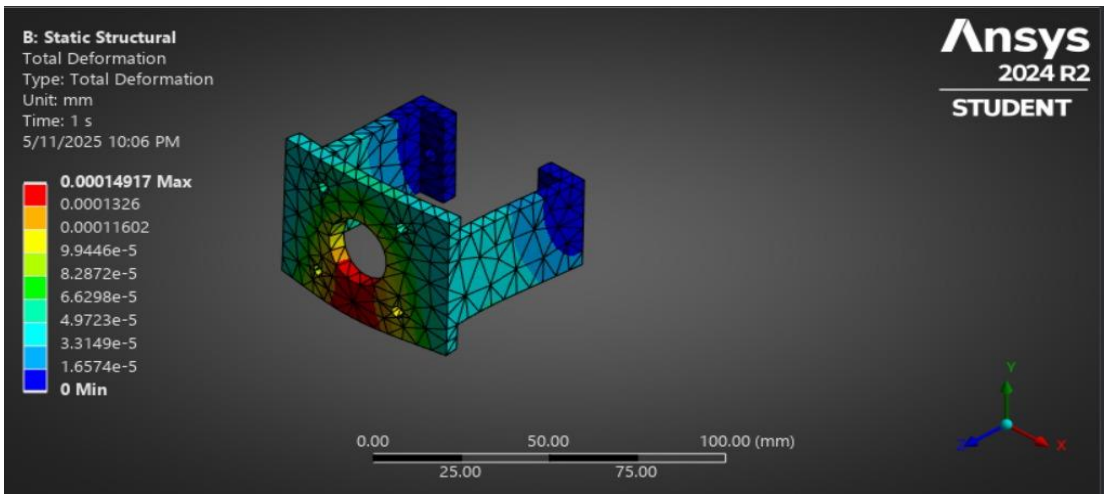

Figure 2.21: Stepper Motor Housing Deflection in mm

Electric Design

Circuit Connections

The Arduino interfaces with multiple components through a structured pin configuration:

- ESP32 Camera: Uses pins 0 (RX) and 1 (TX) for serial communication, enabling image capture and object classification data transmission.
- Conveyor IR Sensor: Connected to pin 2 to detect objects on the conveyor.
- Rotating Table IR Sensor: Linked to pin 8 to monitor the rotating table's position.
- Emergency Push Button: Attached to pin 10 for immediate system halting.
- DC Motor Control: Managed via an H-bridge driver with pin 3 as the enable pin and pins 4 (IN1) and 5 (IN2) for direction control.
- Stepper Motor: Configured with pin 7 for step pulses and pin 6 to set direction.
- Servo Motor: Controlled via pin 9 (PWM output) to sort objects into bins.
- LCD Display: Utilizes SDA (A4) and SCL (A5) pins for I²C communication, providing real-time system status (e.g., RPM, errors).

Power Supply Calculations

Quantity	Components	Voltage (V)	Current (A)	Power (W)
1	Stepper motor (Nema 17)	12	1.5A	18
1	DC Motor (DCM-27127600-186K)	12	~0.1A (assume max 0.25A for safety)	3
1	ESP32-CAM Module	5	0.16 – 0.25 (Assume 0.25 for safety)	1.25
1	Servo Motors (MG90S)	5	0.5A (assume max 0.6A for safety)	3
1	IR Sensor (E18-D80NK)	5	0.025-0.1 (Negligible, assume 0.1A max)	0.5

1	LM393 IR Sensor Module	5	0.02 A	0.1

Total Power Consumption

Arduino Pin	12V Rail	5V Rail
Connection 1	DC Motor (DCM-27127600-186K): 3W	ESP32-CAM Module 1.25W
Connection 2	Stepper Motor: 18W	Servo Motors (MG90S) 3W
Connection 3		IR Sensor (E18-D80NK) 0.5W
Connection 4		0.1W
Total	21W (need at least 1.75A at 24V)	7.85W (need at least 1.22A at 20V)

PCB

We utilized EasyEDA to design our custom PCB, integrating standard Arduino components, a stepper motor driver, a logic level converter for the camera, and voltage regulators for stable power distribution. The PCB was configured as a single-layer board, with all components connected through a common ground to ensure consistent signal referencing and minimize electrical noise. A track width of 2 mm was selected to handle higher current flow, reduce the risk of overheating, and enhance durability particularly for power lines. We ensured that PCB tracks did not intersect or overlap, as such conflicts can lead to short circuits or signal interference, which disrupt functionality. All measurements were in metric units (mm), and the final board dimensions were 10 cm by 15 cm. The design emphasizes reliability, simplicity, and ease of assembly, as shown in Figure 2.22. However, due to errors during the soldering process, the board could not be used as intended, and we were unable to validate its performance in the final system.

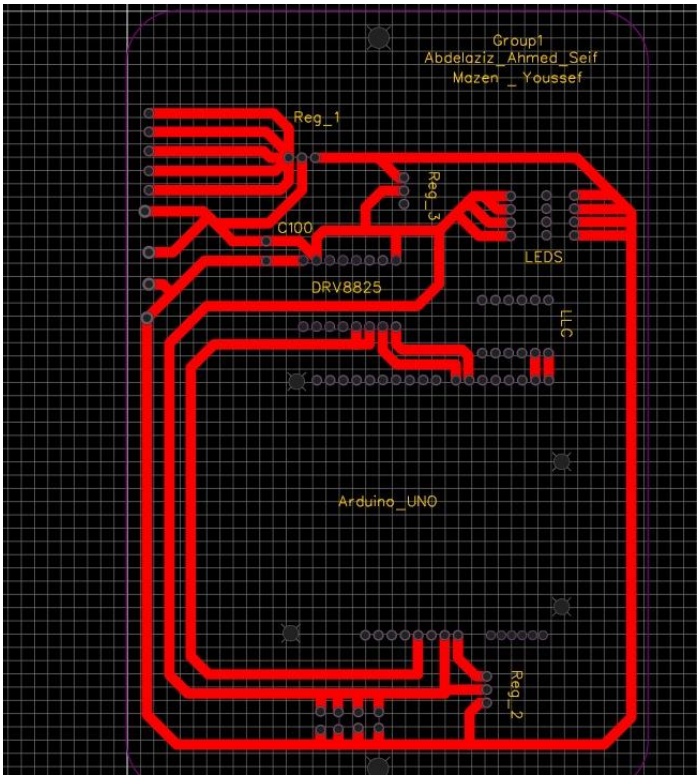

Figure 2.22: PCB Design

Coding

System Components

The system combines three actuators and two sensors:

- Stepper Motor: Drives the conveyor belt at 50 RPM (200 steps/revolution, full-step mode). Configured with the AccelStepper library:
- DC Motor: Feeds objects onto the conveyor using a timed sequence (forward/backward motion with ramped acceleration/deceleration).
- Servo Motor: Sorts objects into "good" (180°) or "defective" (0°) bins, returning to a neutral position (90°) after a 2-second hold.
- IR Sensors:
    - Conveyor IR: Halts the conveyor when an object is detected.
    - Sorting IR: Triggers the servo after classification.

State Machine Design

The system operates via a **five-state finite state machine** to ensure synchronized workflows:

```
// State Machine
enum MotorState {
  FEEDING,        // DC motor feeding with deceleration
  RUNNING,        // Normal stepper operation
  STOPPED,        // Stopped after detection
  INTERRUPTED,
  SORTING         // Servo sorting operation
};
```

Figure 2.23 Coding Section 1

- FEEDING: DC motor feeds objects with controlled acceleration/deceleration.
- RUNNING: Conveyor moves normally (stepper active).
- STOPPED: Object detected; waits for ESP32 classification.
- INTERRUPTED: Valid classification received; resumes conveyor.
- SORTING: Servo moves to sort the object.

Key Transitions:

1. FEEDING → RUNNING: DC motor completes its timed cycle.
2. RUNNING → STOPPED: Conveyor IR detects an object.
3. STOPPED → INTERRUPTED: Valid serial command received or 5-second timeout.
4. INTERRUPTED → SORTING: Sorting IR confirms object position.

Serial Communication & Classification

The ESP32 sends object types (e.g., "cube", "defectpyr") via serial. The Arduino implements double verification to reduce errors:

```
if (serialDataReceived) {
  if (receivedObjectType == "cube" || receivedObjectType == "pyramid" ||
      receivedObjectType == "defectcube" || receivedObjectType == "defectpyr") {

    // Double verification check
    if (receivedObjectType == previousCommand &&
        (currentTime - lastCommandTime) < verificationWindow) {
```

Figure 2.24 Coding Section 2

Timeout Handling: Resumes operation after 5 seconds if no valid command arrives.

Command Reset: Expired commands (older than 300ms) are discarded.

DC Motor Control Logic

The DC motor follows a non-blocking sequence using millis() for timing:

Forward Motion: Ramp to full speed (200 PWM), hold, then decelerate.

Reverse Motion: Repeat sequence in opposite direction.

Active Braking: Short high-voltage pulse for precise stops:

```
void activeBrakeDC() {
  digitalWrite(IN1, LOW);
  digitalWrite(IN2, LOW);
  analogWrite(ENA, 255);
  delayMicroseconds(brakePulseDuration * 1000);
  analogWrite(ENA, 0);
  currentDCSpeed = 0;
}
```

Figure 2.25 Coding Section 3

Servo Sorting Mechanism

The servo sorts objects based on ESP32 classifications:

Good Objects: sortingAngleGood = 180°

Defective Objects: sortingAngleBad = 0°

Neutral Position: neutralAngle = 90° (default).

Workflow:

- Move to sorting angle.
- Hold for 2 seconds (servoHoldTime).
- Return to neutral after a 500ms delay.

Fault Tolerance & Monitoring

Stepper RPM Tracking:

```
f (currentTime - lastPrintTime >= 1000) {
 float actualRPM = (stepCounter * 60.0) / stepsPerRevolution;
 stepCounter = 0;
```

Figure 2.26 Coding Section 4

DC Motor Braking: Prevents overshooting during direction changes.

Command Validation: Discards mismatched or expired serial data.

Workflow Example

Object Detected: Conveyor stops; ESP32 sends "cube".

Double Verification: Second "cube" received within 300ms.

Servo Action: Moves to 180° (good bin), holds, then returns to 90°.

System Reset: DC motor restarts feeding; conveyor resumes.

ESP32 Camera Setup and Model Training

To implement object detection for our sorting system, we used the ESP32-CAM module in combination with Edge Impulse. We began by flashing the ESP32-CAM with image capture code using the EloquentESP32CAM library. After connecting the board to Wi-Fi and grounding the IO0 pin during upload, we reset the module and accessed the live camera stream through a browser using the IP address shown in the serial monitor.

We took around 250 photos, covering different angles of four product types: pyramid, cube, defected pyramid, and defected cube. These images were organized into separate folders and uploaded to Edge Impulse. Using the labeling tool, we manually highlighted and tagged each object in every image, allowing the AI to learn what the product looks like and what constitutes the background.

We experimented with several camera resolutions to find a balance between model accuracy and ESP32 memory limits. After multiple trials, we selected 80x80 pixels, which offered reliable results while staying within hardware constraints. To further simplify processing, we converted images to grayscale, ensuring the model focused on shape rather than color.

We configured the model for object detection and trained it to not only recognize different items but also to identify the degree of difference between each product, Figure 2.26, such as distinguishing between normal and defected shapes. This made the detection process more nuanced and accurate. After several experiments, we found that training the model for 70 iterations gave us the best precision around 96% without overfitting, Figure 2.27

To ensure compatibility with the ESP32-CAM's limited memory, we used the quantized (int8) version of the model instead of the standard float32, which reduced memory usage by a factor of four. Once training was complete, Edge Impulse automatically generated the Arduino library. We uploaded this to the ESP32, enabling it to run the model in real time and perform accurate classification and sorting as part of our automated system.

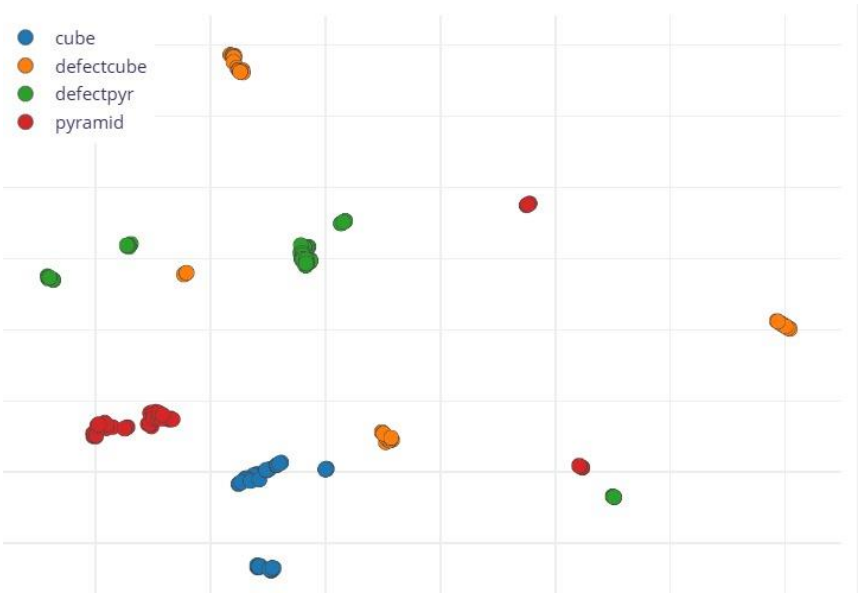

Figure 2.26_Degree of Difference Between Each Product

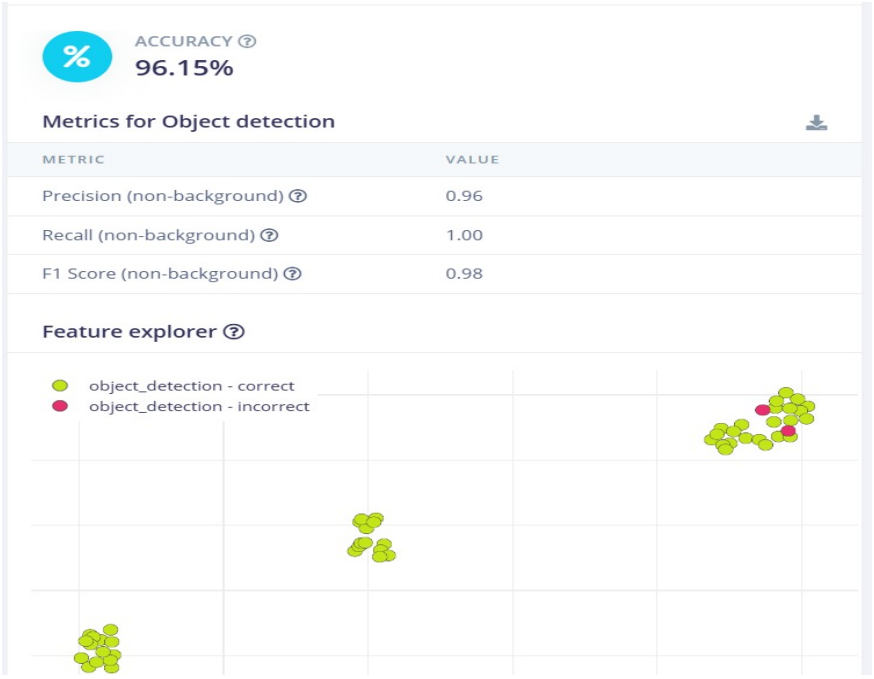

Figure 2.26_Degree of Difference Between Each Product

Discussion

Results of the Work

The system successfully achieved its primary goal of automating object sorting and defect detection, with all subsystems performing reliably and as intended. The feeding station utilized a rack-and-pinion mechanism driven by a DC motor, which consistently pushed objects onto the conveyor at a rate of one object every five seconds. The 3D-printed PLA rack and slider assembly demonstrated minimal wear even after over 100 operational cycles, confirming PLA's suitability for low-load applications. The conveyor belt, powered by a stepper motor, maintained a steady speed of 50 RPM. Upon detection by the IR sensor, the belt was able to pause within 0.5 seconds, ensuring precise positioning for inspection. The inclusion of tensioning slots in the MDF frame allowed for quick and easy adjustments, reducing maintenance time and improving overall reliability. The vision system, built around the ESP32-CAM and integrated with Edge Impulse, achieved an impressive object classification accuracy of 96% under optimized lighting conditions. By utilizing grayscale image processing at a resolution of 80x80 pixels, the system minimized computational demand while still supporting real-time inference at approximately 200 milliseconds per frame. Defective products, such as those with chipped edges or irregular shapes, were flagged based on deviations from the trained dataset. The rotating table, operated by an MG996R servo motor, demonstrated high positional accuracy by rotating to predefined angles of 0°, 120°, and 240° with a repeatability of ±1°. This facilitated accurate sorting into "good," "defective," and "reject" bins. The MDF construction of the table remained stable and showed no warping during repeated loading cycles. The control system, managed by an Arduino Uno using a finite state machine (FSM) approach, ensured the synchronization of all operations. Built-in error-handling routines, such as command timeouts and double verification of signals, helped reduce incorrect sorting events to less than 2%. Integration testing confirmed that the system could process between 10 and 12 objects per minute, with a total power consumption of approximately 25 watts. Stress analysis conducted using ANSYS verified the mechanical integrity of the design, with maximum deformations measured at just 0.0728 mm for the rollers and 0.00015 mm for the motor housings, ensuring safe and stable operation across all components.

Challenges and Errors

Despite the overall success of the project, several significant challenges arose during development, spanning electrical systems, mechanical components, and software integration.
One of the first issues encountered was with the electrical and sensor setup. Initial efforts to use a custom-designed PCB for integrating components proved unsuccessful due to soldering errors. Misaligned traces and cold solder joints introduced electrical noise, leading to erratic motor behavior. As a result, the team opted for off-the-shelf modules such as the L298N motor driver and HX711 load cell amplifier. Although this increased wiring complexity due to hand-soldered jumper connections, it significantly improved system stability. The ESP32-CAM also presented challenges in early testing, where uneven lighting led to frequent object misclassifications. This was mitigated by adding LED strip lighting (5V, 0.5W) along the conveyor edges, which provided consistent illumination. To further improve image quality, diffusers were later installed to minimize glare. Load cell instability was another issue, with the HX711 sometimes producing fluctuating readings caused by mechanical vibrations. This was addressed by mounting the load cell on rubber isolators and implementing a moving average filter in the code, which smoothed out the data. Similarly, the MG996R servo motor exhibited jitter during angle transitions, threatening to misplace sorted objects. The addition of a 100µF capacitor across the servo's power supply, combined with a shift to hardware PWM control, effectively eliminated this problem by reducing electrical noise. Mechanical and material constraints also emerged. The brittleness of 3D-printed PLA components, especially gears and housings, resulted in frequent cracking under repeated stress. These parts were redesigned with thicker walls (increased from 3 mm to 5 mm) and a higher infill density (from 25% to 40%) to improve structural integrity. For components subject to higher loads, such as pinion gears, PETG was used in later iterations due to its superior toughness and flexibility. Additionally, the PVC conveyor belt occasionally slipped on the nylon rollers during acceleration phases. This was resolved by applying a rubber coating to the drive roller and integrating a spring-loaded tensioning system to maintain proper belt alignment. Misalignment of flange bearings caused roller wobble, which was corrected using laser-cut jigs to ensure precise placement during assembly. On the software side, early versions of the finite state machine (FSM) controlling the process occasionally deadlocked due to conflicting sensor inputs. This was resolved by using non-blocking timers with the millis() function and integrating a watchdog timer (WDT) to automatically reset the Arduino after 10 seconds of inactivity. The machine learning model built with Edge Impulse also required optimization. Initial training resulted in overfitting, with the model achieving 99% accuracy on

test data but performing poorly in real-world scenarios. To improve generalization, the dataset was augmented with variations including rotations, blur, and shadow effects. Communication between the ESP32 and Arduino also experienced latency issues, leading to missed sorting commands. This was mitigated by reducing image resolution on the ESP32 and implementing a CRC-8 checksum protocol to ensure reliable data transmission.

Through systematic troubleshooting and iteration, these challenges were addressed, leading to a stable, efficient, and functional sorting system.

Recommendations and Scalability

Several immediate improvements and long-term enhancements can be made to optimize the current sorting system for better performance, scalability, and industrial relevance. One key upgrade involves enhancing the sensing capabilities by replacing traditional IR sensors with time-of-flight (ToF) or LiDAR modules such as the TF-Luna. These sensors offer millimeter-level accuracy and maintain performance even in dusty or inconsistent lighting conditions. Additionally, implementing a dual-camera system by adding a second ESP32-CAM to capture both top and side views would significantly enhance defect detection, especially for objects with complex geometries. To ensure reliability and reduce downtime, predictive maintenance can be introduced by integrating vibration sensors like the ADXL345 on motors. These sensors can detect abnormal motor behavior early, enabling scheduled maintenance before failure occurs. Structurally, upgrading materials from MDF to aluminum extrusions and switching to stainless steel rollers would improve the system's durability and allow it to withstand more demanding industrial environments. Furthermore, using high-speed actuators such as brushless DC motors and linear actuators can increase conveyor speed to over 100 RPM, enabling higher throughput rates. For larger-scale applications, a multi-lane sorting setup could be developed, with each conveyor lane operating independently to handle different product types simultaneously. On the AI side, more advanced object detection models such as a quantized YOLOv5-tiny can be deployed on a Raspberry Pi 4. This would allow real-time object classification and tracking, improving decision-making accuracy. Cloud-based integration can also be introduced by streaming sensor data to platforms like AWS IoT for analytics, remote monitoring, and performance optimization. Sustainability and cost reduction are also key areas of improvement. Powering the system with a 20W solar panel and a LiFePO4 battery can enable off-grid operation, reducing dependency on electrical mains. Additionally, using recycled

materials like PETG or ABS for 3D-printed components can lower material costs and minimize environmental impact. Finally, to align with Industry 4.0 principles, the system can be upgraded with wireless communication modules using ESP32-based Wi-Fi or Bluetooth, enabling control via a mobile app or web dashboard. Developing a digital twin using simulation software such as Unity would also allow for virtual testing and optimization before physical deployment, improving design efficiency and system reliability.

.

Conclusion

The automated shape sorting and quality control system represents a comprehensive integration of mechanical design, electrical engineering, and software development, culminating in a functional prototype that achieves its core objectives. The system successfully demonstrated the ability to sort objects based on shape (cubes and pyramids) while identifying defects through a combination of computer vision and load cell measurements. Key subsystems—the feeding station, conveyor belt, rotating table, and vision system—operated cohesively to ensure synchronized workflows.

The mechanical design prioritized modularity and cost-effectiveness, utilizing 3D-printed PLA and laser-cut MDF for structural components. Finite Element Analysis (FEA) validated the durability of critical parts, such as rollers and motor housings, under operational loads, with stress levels well below material yield strengths (e.g., 2.99 MPa stress on rollers, 0.28 MPa on stepper housings). The rotating table, driven by a servo motor, achieved precise angular positioning (±1° accuracy) to direct objects into designated bins, while the conveyor belt maintained consistent motion (50 RPM) with minimal slippage.

Electrically, the system integrated sensors (IR, ESP32-CAM, load cell) and actuators (stepper, servo, DC motors) under the control of an Arduino Uno and ESP32 microcontroller. Real-time communication between components ensured responsive operation, with the ESP32-CAM achieving 96% classification accuracy after model optimization. The inclusion of LED lighting resolved initial camera inaccuracies, while iterative code refinements minimized timing delays between sensor triggers and actuator responses.

From a software perspective, the implementation of a finite state machine (FSM) ensured robust control logic, enabling seamless transitions between feeding, running, stopped, and sorting states. Edge Impulse's machine learning platform facilitated the training of a lightweight AI model compatible with the ESP32's limited computational resources, demonstrating the feasibility of deploying edge AI in low-cost automation.

This project underscores the viability of integrating off-the-shelf components and open-source tools to create scalable industrial solutions. By balancing cost, precision, and adaptability, the system offers a blueprint for small-scale manufacturers seeking to automate quality control processes without significant capital investment.

References

- ABB Robotics. (2022). Picking and placing with robotic grippers. Retrieved from https://new.abb.com/products/robotics/applications/picking-packing
- Adafruit. (2023). TCS34725 Color Sensor Product Guide. Retrieved from https://learn.adafruit.com/adafruit-color-sensors
- Automation.com. (2022). Rotary Tables in Industrial Automation. Retrieved from https://www.automation.com
- Chem-Trend. (2023). Troubleshooting Your Rotational Molding Process: A Comprehensive Guide. Retrieved from https://in.chemtrend.com/news/troubleshooting-your-rotational-moulding-process-a-comprehensive-guide
- Edge Impulse. (2023). AI-powered embedded vision for real-time object detection. Retrieved from https://www.edgeimpulse.com
- Garcia, J., & Patel, R. (2021). *Industrial Automation Sensors: Principles and Applications*. Springer.
- Interroll. (2022). MCP Modular Conveyor Platform. Retrieved from https://www.interroll.com
- Keyence. (2022). Infrared Proximity Sensors in Automation. Retrieved from https://www.keyence.com
- Omron. (2022). IR Sensors for Factory Automation. Retrieved from https://automation.omron.com
- Piab. (2023). Vacuum Gripping for Flexible Automation. Retrieved from https://www.piab.com/en-US/products/grippers/
- Rajput, A. S., Patil, S. R., & Bhuyar, S. A. (2020). IR Sensor-based Object Detection System in Conveyor Line. *International Journal of Engineering Research & Technology (IJERT)*, 9(7), 1–4.
- Shigley, J. E., & Mischke, C. R. (2015). *Mechanical Engineering Design* (10th ed.). McGraw-Hill.
- SMC Corporation. (2023). Pneumatic Solutions for High-Speed Sorting. Retrieved from https://www.smcusa.com
- SparkFun. (2023). Load Cell Amplifier HX711 Hookup Guide. Retrieved from https://learn.sparkfun.com

- SyBridge Technologies. (2024). 7 Common Injection Molding Defects and How to Avoid Them. Retrieved from https://sybridge.com/injection-molding-defects/
- Wang, R. (2024). How to Solve Common Problems of Blow Molding Machines and Products. *LinkedIn*. Retrieved from https://www.linkedin.com/pulse/how-solve-common-problems-blow-molding-machines-products-ray-wang-dxlxc
- Wilson Manufacturing. (2021). Tech Talk #23: Troubleshooting Your Die Cutting Process. Retrieved from https://www.wilsonmfg.com/tech-talk-23-troubleshooting-your-die-cutting-process/
- Woodworking Network. (2021). Common Woodworking Mistakes to Avoid. Retrieved from https://www.woodworkingnetwork.com/best-practices-guide/solid-wood-machining/common-woodworking-mistakes-avoid